UNIVERSITAT POLITÈCNICA
DE CATALUNYA
BARCELONATECH

Specific energy consumption of metal cutting with thin abrasive discs

Muhammad Rizwan Awan

Specific Energy consumption of metal cutting with thin abrasive discs

Muhammad Rizwan Awan
Thesis director: Hernán A. González Rojas

21st September, 2021

Department of Mechanical Engineering
Universitat Politècnica de Catalunya

A dissertation submitted to the Universitat Politècnica de Catalunya for the degree of Doctor of Philosophy in Mechanical Engineering

Contents

List of figures

List of tables

Nomenclature

e: Equivalent depth of cut
e_g: Grit depth of cut
e_d : Thickness of cutting disc
e_m: Thickness of material
V_c: Cutting velocity
V_f : feed rate
V_{ch} :Velocity of chip
Q_g: Material removal rate with grit
SEC: Specific energy consumption
SEC_{pl}: Specific energy consumed in ploughing
SEC_{pr}: Specific Energy Consumed in primary rubbing
SEC_{sr}: Specific Energy Consumed in secondary rubbing
SCE: Specific cutting energy
P_m: Mechanical Cutting Power
P_{pr}: power consumed by primary rubbing
P_{ps}: power consumed by secondary rubbing
P_{pl}: power consumed by ploughing
P_c: Power of chip formation
C_{pr}: Coefficient of primary rubbing energy
C_{sr}: Coefficient of secondary rubbing energy
C_{pl}: Coefficient of plowing
C_{sl}= Coefficient of sliding
ρ= Density (kg/m^3)
C_p: Specific heat capacity(KJ/kg.K)
L: latent heat capacity (KJ/Kg)
α:Rake Angle
Φ:Angle of cutting plane
h: Shear band thickness (mm)
u_o: Horizontal component of velocity at the entrance of band
u_1: Horizontal component of the velocity at the exit of the band
V_o: vertical component of the velocity at the entrance of the band
V_1:Vertical component of the velocity at the exit of the band
$\dot{\gamma}$: Shear Strain rate
$\dot{\gamma}_s$: Maximum Shear Strain rate

Foreword

The aim of this research is to provide an in-depth understanding of energy consumption in abrasive disc cutting processes. The specific energy consumed in cutting is measured, analysed, and then characterised in to three components. To this end, an experimental device is built using an Arduino-controlled grinder to measure the specific energy consumed by cutting at different feed rates. Using a model, the experimental data is validated and the Specific Energy Consumed is separated into three energy components: sliding, ploughing and specific cutting energy.

Furthermore, the influence of cutting conditions and material properties significantly influenced the specific energy consumption and its components. To analyse the effect of grain shape and the relative dependence of the different components of the Specific Energy Consumed as a function of material removal rate, integral models of specific ploughing energy, specific sliding energy and specific cutting energy are developed. Conventional and super abrasive cubitron abrasive grains were used. Cutting with pyramidal abrasive discs (cubitron) was used for the determination of the relative components of the specific energy consumed. It was found that the specific ploughing energy is more sensitive to the change in material removal rate compared to the sliding energy. Due to the fast shearing and precisely shaped cubitron grains, the transition from sliding to a specific shear regime was so fast for some materials that the magnitude of the ploughing energy was found to be negligible. However, the model implementation for some materials showed that the absence or presence of ploughing energy also depends on the rate of material removed.

Finally, the development of a cutting grain model is presented which will allow the study of the chip compression ratio which is not possible to characterise by means of a single cutting grain in metal cutting with thin abrasive discs. This latest development is the beginning of a study of chip formation in the primary cutting zone of an abrasive grain. This research provides a machine and a methodology to characterise cutting with commercially available abrasive discs in terms of the Specific Energy Consumed parameter.

Acknowledgement

My quest for doctorate is motivated by my curiosity to analyze the challenging problem from a different perspective. I believe that the mental aptitude developed during this journey to tackle unknown problems will help me a long way to undertake practical research in the future.

To achieve this milestone, I will always be indebted to the strong support and commitment of some personalities. First of all, I pay highest gratitude to my supervisor and professor, Hernan Gonzalez Rojas for considering me and believing in me. His support, commitment, and active supervision has been remarkable during this whole journey. I am highly inspired by his critical thinking skills, way to understand the problem, and style of conveying it to the student. For me, his doors were always open and he went out of the way to help me, whenever I needed. He played significant role in developing my research and critical thinking skills and helped me in my transformation to a better research student.

The other personality, to whom I pay profound regards, is my great friend Saqib Hameed. He stood beside me during this whole journey, and made it possible for me to sustain in challenging circumstances. For three continuous years, he remained persistent in easing my out of school burdens. Without his help, it would not have been possible for me to pursue this journey.

My respected parents, who are my inspiration, always supported me throughout my whole life. Through their sincere efforts, encouragement and support, I have reached this far and been able to complete my doctorate. My brother, and sisters remained my great moral support during this journey.

Last but not the least, my wife played very positive and active role to always encourage me and stood behind me during this time. Through her support, I was able to focus on my PhD, despite many challenges.

Chapter 1 Introduction

1.1 Abrasive processes

Abrasive machining processes are metal cutting operations involving hard, sharp and friable, small-sized particles called abrasive grains (grits) which act as cutting tools. The most widely used grits are silicon carbide, aluminum oxide, synthetic diamond and cubic boron nitride. The common industrial abrasive processes are grinding, honing and lapping with grinding being the best known and the most commonly used [1]. In grinding, a cutting tool of high abrasive surface is made in contact with work piece resulting in material removal from both the abrasive and the work piece. Traditionally, grinding has been used as the précised finishing process, to produce the parts with closed tolerances and to fine the surface finishes [2]. Grinding processes vary according to the shape of the wheel and the kinematics of motion of the work piece and wheel head[3]. The cutting properties of the disc are predominantly defined by the properties of abrasives but also by the bonding agent, the fillers and the reinforcement fabric [4].

1.1.1 Abrasive cut off operation

Grinding, being a very complex material removal mechanism, is broadly classified in to the two categories namely finish and form grinding (FFG) and stock removal grinding(SRG)[5]. Cut-off operation is a stock removal grinding (SRG) process where the emphasis is on the removal rate than on generating required finish and accuracy, as in form and finish grinding (FFG) [6]. It is the sectioning of material, using a relatively thin rotating disc composed of abrasive particles supported by a suitable media [7]. In finish and form grinding (FFG), fine grain sized conventional abrasives like (alumina, SiC) are used, and wheels are periodically dressed. In SRG coarse grain size abrasives are used in resin bonded grinding wheel and wheels are sometimes reinforced with fiber glass to avoid fatal accidents during the operation. Cut off wheels are used without being dressed, and in comparison to surface grinding, wheel speed is generally higher. In surface grinding, abrasive wheel reciprocates with specific depth of cut in relation to work piece, where as in abrasive cut off operation, cutting wheel is fed radially in to the work piece at a given feed rate. Unlike surface grinding, abrasive cutting off operation is usually conducted in dry conditions, as water can reduce the life of cutting wheel [8].

In comparison to conventional grinding operations, studies on abrasive cut off operation are a few. Most of the research on abrasive cut off operation was started in late 1960s by Prof. Shaw [9]. He evaluated the mechanics of abrasive cut off operation in great detail. In another study [10], he introduced the criteria to rate the cut off wheels on the basis of number of active cutting

points, the void space between the successive grains, and feed rate in relation to grinding ratio. Eshghy [11] analyzed the thermal aspects of abrasive cut off operation in relation to the energy required to remove the unit volume of material. Zheng and Ranga[12] presented the new thermal model for abrasive cut off operation. In contrast to previous model, which took the area of contact between wheel and work piece, this model considered the actual area of contacting grains as the heat source on work piece and wheel interaction. Heat flow at the time of interaction between work piece and wheel was found to be one dimensional.

As metal cutting with abrasive discs is also a phenomenon of material removal through abrasive grains, so specific energy, forces, material removal and other factors are governed by the same principles as grinding. As discussed earlier, research on grinding is well established, so in this project the grinding literature is extensively discussed to better understand abrasive cut off operation in terms of cutting conditions and specific energy consumption.

1.1.2 Grain properties

The material of the grit, its shape and characteristics of the contact between the grit and the bonding agent is of great significance for analysis of abrasive processes[4]. The grain size and shape influence the grinding force, specific energy and tool life[13]. Studies of single grit interaction with work piece enable to understand the material removal mechanism in grinding[14]. Malkin et al. [15] statistically analyzed the abrasive grits on grinding wheel and postulated that rack angle of grits is highly negative, and an average size of grinding grit is -60^{o}.

Rowe[16] determined the way to represent the grain sharpness by drawing a circle through the extremities of contact with work surface. The measure of the sharpness of the contact is represented by depth to diameter ratio t/d. It can be seen in Figure 1 that a sharp grain easily cuts the work piece, and a blunt grain with wear flats consumes more energy as sliding or rubbing energy. Increase in grain depth, makes the effective rake angle less negative so grain sharpness increases. Grain sharpness, therefore, is an indicator for the explanation of size effect.

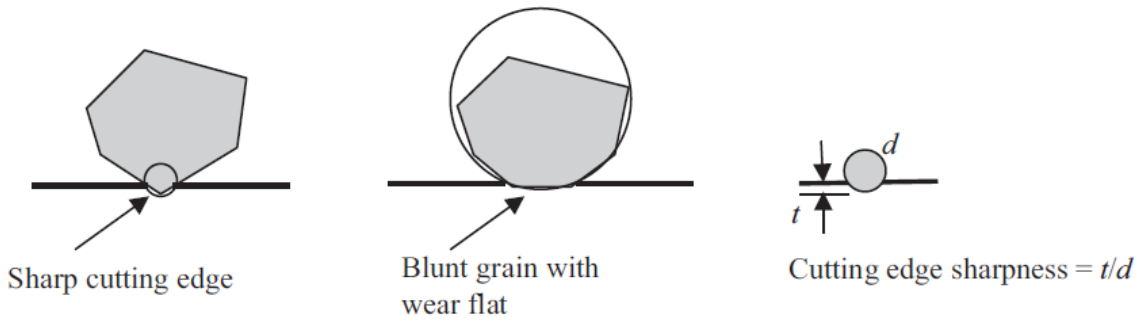

Figure 1 Effect of grain shape on material removal mechanics

Shaw [17] presented the indentation model of the grain to analyze the energy required to deform the material. The applied force to grain was considered similar to the force applied in hardness test. With the indentation of the grain in to the work piece, the region becomes plastic, and flows sideways and upward around the grain as shown in figure 2.

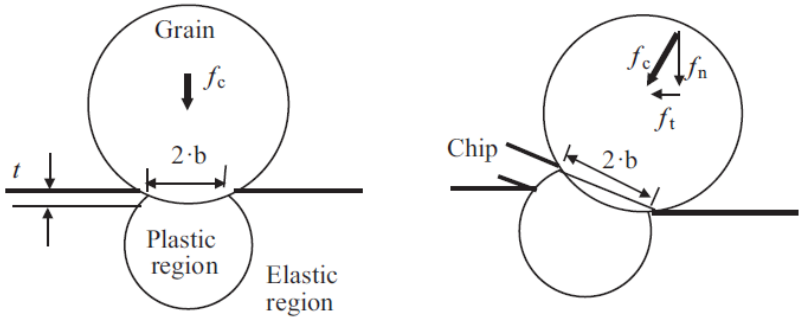

Figure 2 Indentation model of grain

According to this model, specific energy depends on hardness of the material, plowing, friction at the interface, and grain size and grain depth of cut. Reducing the grain depth t increases the specific energy. The size affect evaluated on the basis of grain spherical model is directly dependent on the grain sharpness, as increasing the depth t, increases the grain sharpness and reduces the specific energy.

Takenaka[18] was only of the earliest researchers to perform scratch test and observed that chip produced in the form of torn leaves mainly by cutting phenomenon, when the depth of cut was higher than 1um. He also found the plowing energy as predominant form of energy dissipation at low depth of cut. Recent research indicate that orientation of grain plays a significant role in energy dissipation and material plowing rate[19]. Rasim et al[20] presented the single grit scratch method to physically investigate the chip transition stage. The 3D grain geometry was investigated with respect to apex angle, rake angle, grit cutting depth and the effect of these parameters on material removal phases and chip formation was analyzed. He evaluated that chip formation in grinding is significantly influenced by the grain shape in direction of motion as well as in transversal direction. Buttler et al.[21] investigated the influence of grain shape on the material removal behavior of brittle and ductile materials. They evaluated that specific cutting force of brittle materials is reduced with increased number of cutting edges on the grit surface, while in case of ductile materials the specific cutting force increased with increasing the contact area between grit and work piece specimen. Tahsin et al. [22] investigated the influence of grit shape on grinding efficiency and quality during material removal mechanism. They evaluated that grit cutting edge has significant influence on plowing and cutting action and single edge grit proved to be more efficient than multiple edge grits.

1.1.3 Number of active cutting grits

The number of active grits per unit area is an important parameter in grinding operation. As grinding is the stochastic process and all the grits do not participate in material removal process, so number of active cutting grits is a concern for researcher. Becker and Shaw[9] were the amongst the early researchers who attempted to determine the number of active cutting grits by rolling the grinding and cut off wheels on glass plate coated with smoky flame and sanborn recording papers respectively. By counting the printed number of contacts per square inch on glass plate and sand paper provided the number of active cutting grits. Later on, many researchers developed different models to predict the active number of cutting grits. Setti et al[23] developed a method to predict the active cutting grits by assuming the stochastic distribution of grits. The effect of process parameters like depth of cut, grit size, and work piece hardness was also considered. Jamshedi et al. determined the active number of grits by developing kinematic equations which are influenced by the parameters of grit height distribution, grinding condition and wheel vibration[24]. Pang et al [25] used the embedded grindable thermocouple to investigate the active number of cutting grits. The thermocouple was used to detect the dynamic variation of temperature signals, which reflected the variation of wheel topography under different process parameters. They evaluated that active grit number is about one fourth to one third of static grit. Active number of grits increased with increasing depth of cut and work piece speed and by decreasing the wheel speed.

In comparison to grinding, a very few studies have been directed to count the number of active cutting grits in abrasive cut off operation. Zhen and Ranga [12] determined that out of large number of grains only 18% are contacting grains for 46 grit size and 10.8% for 24-grit size. Out of these contacting grains, 1.75% are actual cutting grains for 46 grit size and 1.6% for 24 grit size.

1.2 Energy consumption in Grinding

Today, industrial sector is responsible for 85% of the energy used in the world, with manufacturing accounting for 40% of the energy used in the industry [26]. Low energy consumption is amongst the greatest challenges of manufacturing industry to minimize environmental impact and reduce the production cost [27, 28]. Machining is one of the most important manufacturing technologies and it also represents the major energy demand [29]. Energy consumption estimation and understanding is the first and important step to reduce the energy consumption of the machining [30]. Specific energy consumption i.e., the energy required to remove the unit volume of material (SEC), is an important metric to evaluate the energy consumption of machining [31]. In terms of specific energy consumption, grinding is one of the highly energy intensive process amongst other metal cutting operations. In grinding, the largest portion of emissions is attributed to the energy used in material removal [32]. The

grinding process, which emphasizes on the high material removal is the abrasive cut off operation, it is the sectioning of materials with thin cutting discs made of abrasive particles [7, 33]. So, specific energy analysis of grinding process involving high material removal is of great significance.

1.2.1 Three Energy components

The material removal mechanism in grinding on micorscale was first analysed by Hahn and proposed the three material removal regimes with their corresponding energy components[34]. The SEC of grinding has three components, consisting of chip formation energy, plowing energy of material deformation and sliding or rubbing energy [13].

$$E_s = E_{sl} + E_{pl} + E_{ch} \quad (1)$$

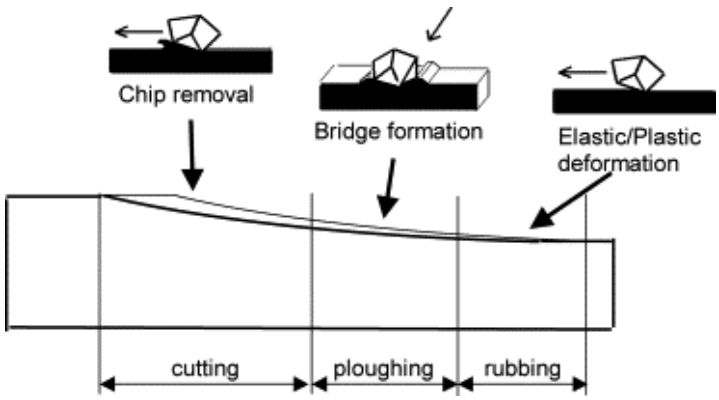

Figure 3 Grit work piece interaction

1.2.1.1 Sliding or Rubbing Energy

Rubbing or sliding is the first stage of grain interaction with work piece; elastic deformation takes place in this phase with negligible amount of material removal[35]. According to Rowe[16], sliding energy increases with increase of wear flats areas. For sharp wheels, there are no wear flats, so specific energy consists only of plowing and chip formation energy. Malkin's [36] work on surface grinding for materials of AISI 52100, 130A Ti and SAE 1018 also show that normal and tangential forces increases in proportion to grain wear flat area.

1.2.1.2 Primary and Secondary Rubbing Energy

Recent studies on abrasive grit workpiece interaction divide the sliding energy in to primary and secondary rubbing energies. Manoj et al.[37] and Singh et al.[38] conducted abrasive grit tests to analyse the sliding and plowing energies. They observed two kinds of rubbing energies while grain contact with the work piece. Figure 4a shows primary rubbing phenomena, as the grit moves in relation to work piece, its original path is AC, but due to bluntness of the grit, it cannot penetrate in to the work piece instantly at A, it rather moves along the path AB. At any position along the path AB, for instance D, the contact stress is developed which is a function of normal force, contact geometry and the radius of curvature of cutting path. If this contact strength is higher than the strength of the material, then the grit tip would penetrate in to the material.

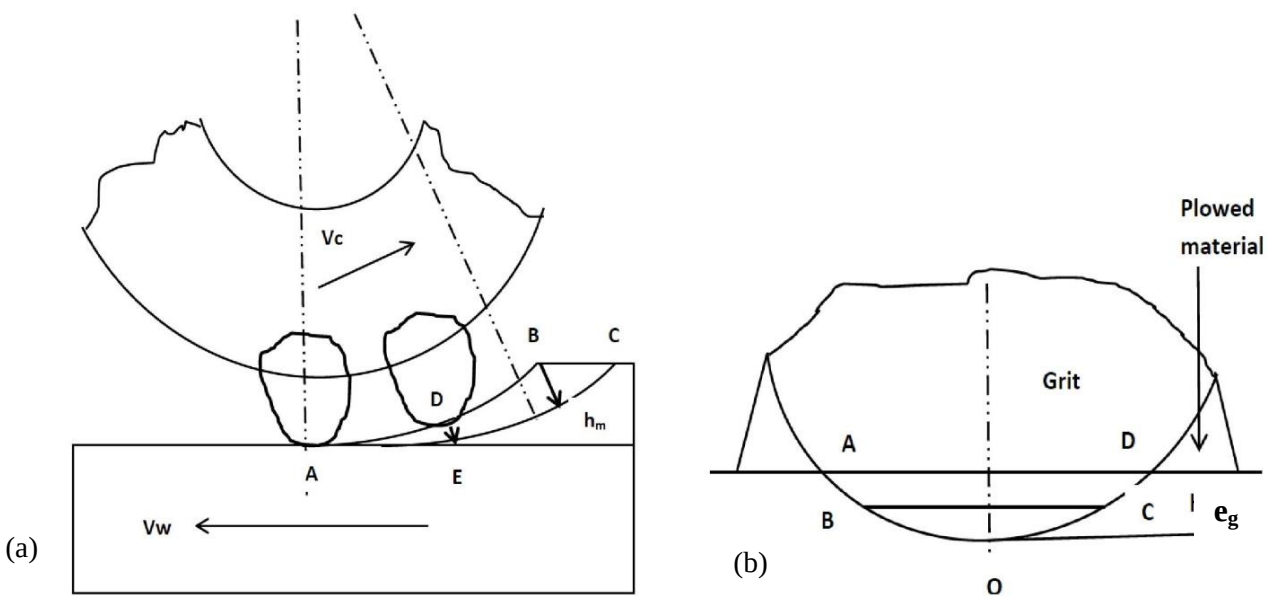

Figure 4 Primary and secondary rubbing energy (a) rubbing mechanism of grit (b) grain profile

So, it can be deduced that actual cutting path is from A to D, followed by grain penetration from D to E and chip formation from E to C. The energy dissipation from A to D due to sliding of the grit is called primary rubbing energy, and it does not participate in the material removal process. Due to negative rake angles of abrasive grits, secondary rubbing energy occurs between the cutting edge and work piece. The grit ribs against the whole cutting profile ABOCD as shown in figure 4b. The rubbing of the grit against the reattachment of the machined material is the main reason for secondary rubbing energy[39, 40].

1.2.1.3 Plowing Energy

After sliding, further increase of force, grain penetration in to the work piece is increased leading to plowing phase, both elastic and plastic deformation take place in this phase. With increase in material removal rate, plowing energy per unit of volume reduces. With increase in depth of cut or feed rate, plowing energy becomes a smaller portion of total energy. This reduction in plowing energy is the main reason for size effect[16]. According to Rubenstein[41], plowing energy is influenced by grit shape, material properties and process parameters. Ghosh et al.[19] and Singh et al.[42] suggested that effective negative rake angles on the leading face of grain significantly increase the plowing energy in single grit grinding and indentation tests. With the increase of grain depth, effective negative rake angle reduces, which reduce the plowing energy.

Researchers adopted different methods to estimate specific plowing energy. Manoj et al[43] analysed the specific plowing energy in single grit tests, and determined that higher pile up ratio at lower feed rates presents more plowing phenomenon. Patnaik et al [44] evaluated the specific plowing force in terms of process parameters for mild steel (SAE 1080) using the single grit test. Matsu et al. [45] used CBN and diamond grits for single grit scratch tests to measure pile up material under different testing conditions. Vijaneder et al.[46] modelled specific plowing energy using single grit scratch test. In their work, grit rake angle and the effect of process parameters were considered. Specific plowing energy was determined as

$$U_{pl} = \frac{f_{tp} V_c}{\mathrm{MRR_{grit}}} \qquad (2)$$

f_{tp}= Tangential force in plowing (N) at grit level
V_c= Grinding Velocity (m/s)
MRR_{grit}= Material removal rate (mm^3)

At the low depth of cut, specific energy of the grinding process is high, this phenomenon is known as the size effect. The concept of specific plowing energy helps to understand the size effect as it is the predominant form of energy dissipation at low material removal rate. The high-specific energies of grinding operation is attributed to the high sliding and plowing energies[42].

1.2.1.4 Chip formation Energy

After plowing phase, further penetration of grain leads to cutting phase, where material is plastically deformed to produce chips [35, 47]. Malkin and Joseph analysed that [48] the chip formation energy is larger than the energy carried away by the chips. The energy carried away by the chips is almost equal to the amount of energy required to melt the material. Based on this, Rowe[16] estimated the energy carried away by the chips as

$e_{ch} = \rho . C . T_{ch}$ Maximum chip formation energy

Where ρ is the material density, C is the average specific heat capacity, and T_{ch} is the average temperature rise of the chips. The chip formation energy remains constant and at very high material removal rate, it is only apparent energy. It is also the minimum energy required to produce chips. This minimum energy for chip is not affected by little alloying or heat treatment.

In machining, the uncut chip thickness is larger in comparison to grinding, so contribution from sliding and plowing energies is negligible, and main form of energy dissipation during deformation is shearing or specific cutting energy[36, 43].

1.2.2 Dominance of specific energy components in grinding processes

Various factors like abrasive sharpness, material properties and process parameters govern the transition of energy consumption behaviour between these three stages and have been extensively discussed. According to Rowe [49], rubbing or sliding is predominant form of energy in material removal for processes like polishing and lapping, whereas precision grinding takes place in all three regimes. High energy deep grinding and cut-off operations take place predominantly in the material removal regime by chip formation for ductile materials or by crack formation for brittle materials.

Researchers developed different models to analyse the dominance of particular energy component. For instance, Napoles et al.[50] developed the material removal rate model to evaluate specific energy consumption during industrial scale grinding of C45K with different thermal treatments and AISI 304. They demonstrated that sliding energy is the main form of energy dissipation, and it decreases with increase of depth of cut. Masoumi et al.[51] investigated the material removal behaviour during surface grinding of high velocity oxy-fuel (HVOF) thermally sprayed WC-10Co4Cr coating. Their research results revealed that material removal is both due to brittle fracture and ductile flow modes depending on grinding parameter variation, and large amount of energy is dissipated by plastic deformation due to plowing. Similarly, Singh et al. [38] found specific plowing energy as most significant component at smaller feed rates for grinding of hard and high strength materials. Shaw[52] demonstrated that in finish and form grinding (FFG), little energy is carried by chips while in stock removal grinding (SRG); most of the specific energy is consumed as shear cutting energy to produce chips. According to Malkin and Joseph [48], at very high material removal rates, sliding and plowing energy become negligible and the minimum energy is equal to specific chip formation energy. This minimum energy to form the chips is constant, and at higher removal rates, it is the only dominant energy [31].

1.3 Estimation of Specific energy for abrasive cut off operation

Accurately predicting the grinding energy is quite difficult as grinding is a complex process, so researcher attempted different models to predict the grinding energy requirement. Singh et al. and Ghosh et al. [19, 38] evaluated on the basis of different models that variation in plowing energy is the main reason for change in specific energy consumption, as sliding energy and specific chip formation energies are constants and have less magnitudes. The prediction of grinding energy however depends on the combined effect of several variables[16]. Rowe concluded that grinding energy variation is a function of several variables like grain sharpness, feed rate, depth of cut, and wheel speed.

Contrary to a lot of research studies on specific energy for finish and form grinding (FFG), specific energy consumption of abrasive cut off operation with thin cutting discs for metals has rarely been discussed. In one of earlier studies, Shaw et al.[9] analysed the influence of feed rate on specific energy consumption and cutting forces in abrasive cut off operation for steel and aluminium. They used cutting disc of large diameter (508mm) and very high feed rates (3.39-12.7mm/s) for the experimentation. Specific energy was presented as the function of ratio of feed rate to wheel speed(d/V), tangential cutting force F_p, width of cut b, and length of cut l.

$$U = \frac{VF_p}{dlb} \tag{3}$$

The results revealed that cutting forces increased with increase in feed rate up to some extent and then dropped down from the trend line. The specific energy consumption decreased with increase in feed rate, however, their study did not explain the three specific energy components of rubbing, plowing and cutting during material removal. Turchetta [53] investigated the cutting conditions that affect the cutting force and cutting energy in stone cutting by diamond cutting disks. His work exhibited that cutting energy decrease with increase of depth of cut and feed rate, while, the cutting force increased with increase of equivalent chip thickness. The adopted model for specific energy in this study did not explain the material removal phases and their corresponding energy components.

In all the previous studies to measure specific energy consumption of grinding and abrasive cut off operation for metals, stone and optical glass cutting[9, 31, 53–55], cutting power has been measured in terms of tangential forces and cutting velocity of the disc as shown in Eq (4).

$$P = F_t V_c \tag{4}$$

This study aims to introduce a new experimental technique to directly measure the cutting power for specific energy evaluation of abrasive cut off operation. For this purpose, state of art experimental set up has been designed and manufactured to perform metal cutting with abrasive discs. A new methodology has been presented which provides an alternative way to measure cutting power which has not been done before. This methodology uses a combination of analytical method and specially designed and manufactured equipment to automate the movement of a standard grinder at different feed rates. In addition, particularly, in studies of abrasive cut off operation, specific energy has not been distinguished into three modes during material removal[9, 56]. In this research, specific energy measured through an alternative method has been characterized into three modes of sliding, plowing and cutting using an empirical model. Moreover, the comprehensive modelling of specific energy consumption helped to determine the relative contribution of specific energy components during material removal mechanism. These three components of sliding, plowing and cutting have been discussed for grinding in the literature review, because grinding also involves metal cutting with abrasive discs and has been extensively discussed and analysed. The research presented below will help to understand that how material properties and cutting conditions affect the behaviour of SEC during material removal.

1.4 Objectives

The main objective of this research is to study the specific energy consumption of abrasive metal cutting with thin discs. The focus of the project is to investigate how process parameters, cutting conditions and material properties influence the specific energy consumption and its corresponding components. For this purpose, a state of art experimental set up has been designed, and manufactured to perform the abrasive metal cutting with thin discs. To achieve the main goal, following are the specific objectives of the research

1. Design and manufacture machine through which metal cutting with abrasive discs can be performed at various feed rates.
2. Devise a methodology to measure the specific energy consumption of different materials.
3. Analysing the experimental data with empirical model to characterize the specific energy consumption in three modes of sliding, ploughing and specific chip formation.
4. To develop the comprehensive models of sliding, plowing and specific cutting energy to understand the influence on material removal rate on specific energy components
5. Develop the model of cutting grain to determine the equivalent chip thickness and most significant parameters for material removal rate.

1.4.1 Scope

The main activities that included in the scope of this research project are

1. Develop the program of microcontroller to operate the stepper motor at different feed rates
2. Design and assemble system components like stepper motor, lead screw and standard grinder
3. Calibrating the standard grinder on the test bench to determine the relationship between effective electric power and mechanical cutting power.
4. Carrying out the simulation to find out the feed rates in relation to stepper motor speed
5. Measuring the mechanical power at different feed rates
6. Estimating the sliding energies with an experimental procedures and calculating the specific ploughing energy and specific cutting energy using empirical models.
7. Development of models for specific energy consumption and its components
8. Heat generation and distribution at the grinding zone has not been considered for this research.
9. The minor vibration of grinding disc during operation has been ignored.

1.5 Thesis Organization

1.5.1 Chapter 2

This chapter reports the methods to estimate specific energy consumption. An alternative methodology to evaluate specific energy consumption has been developed. In addition, the model has been applied to characterize specific energy consumption in to three components of sliding, plowing and cutting. This chapter is article publication in Journal of advanced manufacturing engineering-Springer.

Awan, M.R., Rojas, H.A.G., Benavides, J.I.P. et al. Experimental technique to analyze the influence of cutting conditions on specific energy consumption during abrasive metal cutting with thin discs. Adv. Manuf. (2021). https://doi.org/10.1007/s40436-021-00361-2

1.5.2 Chapter 3

This chapter is an improved model of specific energy consumption. The detailed models of specific plowing energy, specific primary and secondary rubbing energies are presented and validated through experimental data. This chapter is intended to be published in Journal of Manufacturing Processes. Elsevier (IF 5.0)

1.5.3 Chapter 4

In this chapter, single grain cutting model is developed to determine the chip compression ratio and to analyse either cutting velocity or feed velocity is a better parameter to evaluate material removal rate. In the second section, model of shear strain rate has been introduced to better understand the shear strain distribution at the grinding zone.

1.5.4 Chapter 5

This chapter enlists the overall conclusions and provide details about how many different ideas can be further explored based on this research.

Chapter 2

Specific Energy Consumption Estimation

2.1 Methodology to evaluate Specific Energy Consumption

2.1.1 Measurement of Cutting Power

Estimation of specific energy consumption involves measurement of cutting power and material removal rate. As Specific energy consumption is defined

$$SEC = \frac{P_m}{Q_c} \quad (5)$$

The measurement of cutting power P_m in this research work has been done using the combination of two experimental settings. In the first setting, as shown in figure 5a, standard angle grinder is coupled with dynamometer to measure and determine the relationship between mechanical power and electrical power consumed at different loading conditions. The Hysteresis Dynamometer, model HD-710-BNA developed by Magtrol USA has been used for this experiment. A high speed programmable controller attached to dynamometer displays the measurement of mechanical characteristics like torque, mechanical power (P_m), speed of rotation (rpm) and electrical characteristics like effective electric power (E_e), and voltage.

The effective electric power E_e or average power is the power capable of transforming electrical energy into work. Part of the dynamometer equipment is the device that measures the effective electric power. This device does this by multiplying current and voltage instantaneously using a 4-quadrant multiplier and then averages the instantaneous power signal. The mechanical power P_m is defined as the product of torque and angular velocity. The relationship between mechanical power P_m delivered by the grinder and effective electric power E_e consumed by the motor is shown in figure 6. The behaviour of this regression curve is associated with the grinder used and, therefore it is an experimental result of the behaviour of the equipment used. The trend line between these two parameters is linear; Eq. (6) is the regression equation of this trend line and 2.4 denotes the slope of line. Eq. (6) obtained through this graph is particular to this grinder and can be used to find the mechanical power during metal cutting with abrasive disc for repetitive experiments. Using the regression equation to measure the mechanical power through the electrical energy consumed during abrasive cutting with disc, eliminates the need to measure the cutting force, and cutting velocity for specific energy estimation.

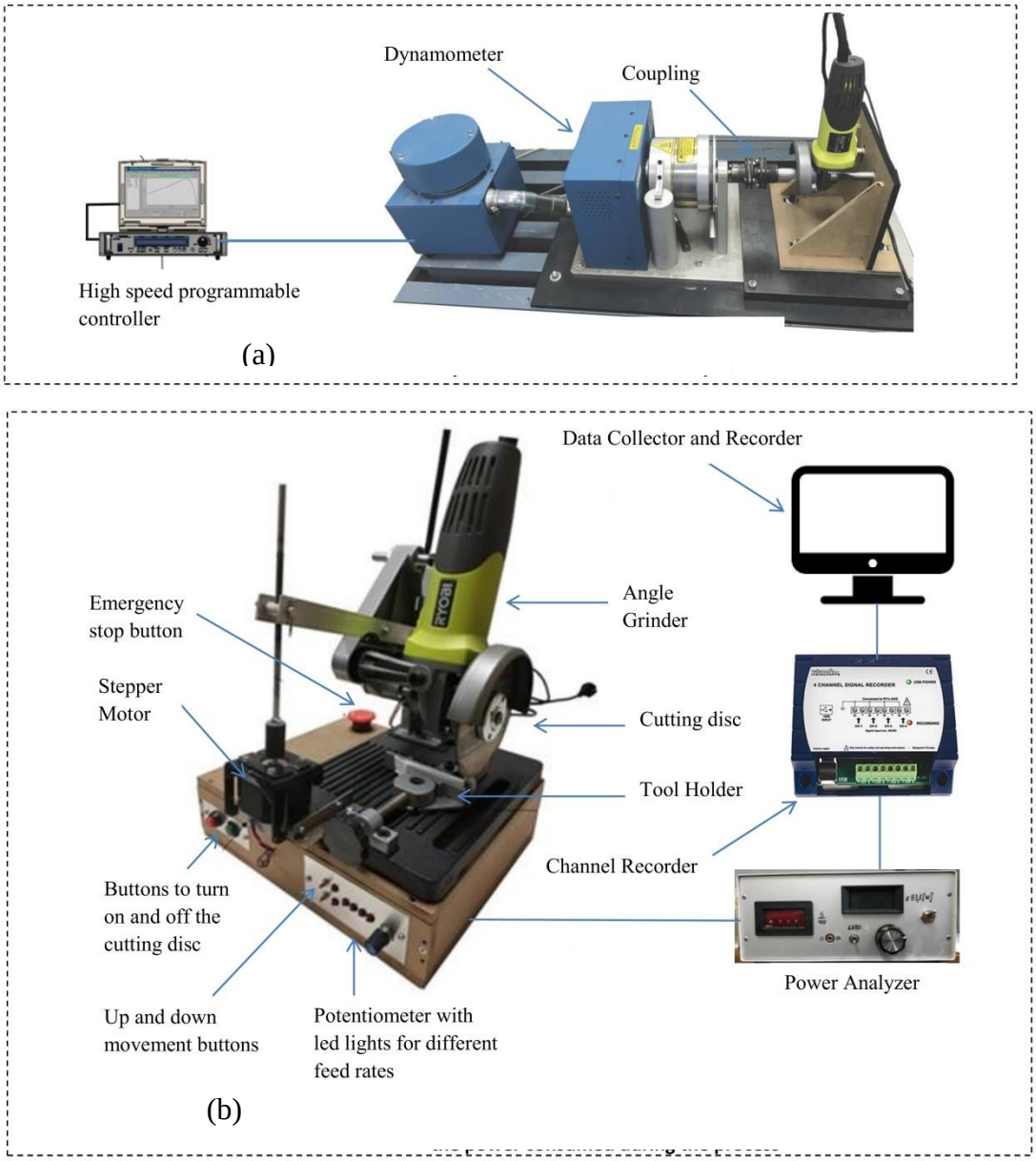

Figure 5. Experimental set up to measure Mechanical Power and SEC (a) standard grinder coupled with dynamometer to measure P_m (b) SEC Measurement on machine

$$P_m = 2.4E_e - 742.61 \quad (6)$$

In the second step, standard angle grinder is mounted on the experimental configuration, which has been specifically designed and manufactured to mount and operate the standard disc grinder on various feed rates for metal abrasive cutting operation studied in this work. Figure 5b, in the second setting, illustrates the different parts of the equipment developed for this study. Ultra-thin disc of 1mm, mounted on the Angle grinder acts as a cutting tool to machine the metallic bars.

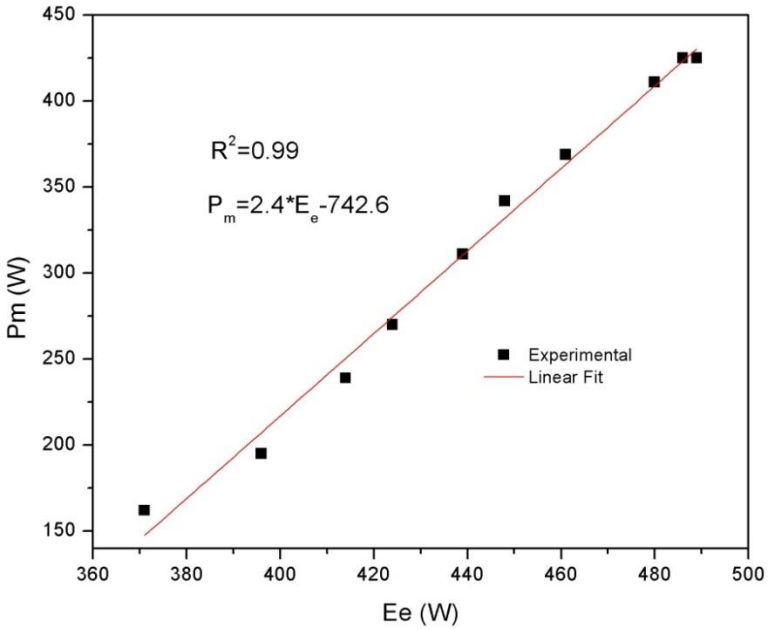

Figure 6. Mechanical Power vs. Electrical Energy

Stepper motor operates the machine on four different feed rates defined by the potentiometer. The LED lights have been used as the indicator of four defined speeds. Two vertical separate buttons have been placed for the clockwise and anticlockwise movement of stepper motor which eventually moves the machine up and down.

2.1.2 Description of Electrical components

The schematic diagram of electrical components inside the wooden box is shown in figure 7. The speed, movement and direction of stepper motor in relation to input feed rate value, have been programmed through microcontroller Arduino Uno. Stepper motor drive TB6600 controls the current between stepper motor and control circuit in micro steps. The feed rate value range can be changed by changing the no of steps in drive. Grinder buttons, emergency stop button and limit switches are controlled through switch relay. Limit switches are programmed with microcontroller, which actuate to stop the stepper motor once the movement reaches the maximum up or minimum down limit on the lead screw.

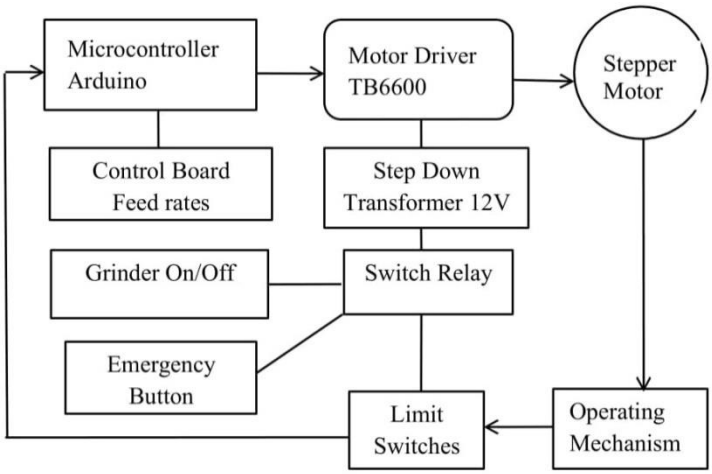

Figure 7. Schematic diagram of electrical instruments

. The power source is used to step down the input voltage supply to 12V for stepper motor drive and other functions. The electrical energy consumed E_e by the machine during cutting off operation is measured through the power analyser at different feed rates, which is stored in computer through the channel recorder. Using these electrical energy values, the corresponding values of mechanical power are calculated through regression line Eq. (6).

2.1.3 Work piece Material and cutting tool

The materials used in this experiment are S235JR, C45K, and ferrous aluminium based inter metallic alloy FeAl (40%), having chemical composition of Fe-60% and Al=40%[57]. C45K is studied in three different states i.e., C45K normal condition, C45K with Quenching and C45K with Quenching plus tempering. The chemical composition of S235JR and C45K is given in table 1.

Metallic Alloys	C	Mn	P	S	Si	Ni	Cr
C45K	0.5	0.50-0.90	0.03	0.035	0.4	0.4	0.4
S235JR	0.22	1.6	0.05	0.05	0.05		

Table 1 Percentage chemical composition of metallic alloys

Metallic Alloys	C45K	C45K-Q	C45K-Q+T	S235JR	Intermetallic
HRB	100.2	120.6	85.85	80.05	100.2

Table 2. Material Hardness

The Hardness of materials (HRB) given in table 2, is measured with Rockwell hardness tester (developed by Wilson), with indenter load of 100 kg. The abrasive cutting action is performed by ultra-thin steel cutting disc of 1mm thickness; 22mm bore diameter and 115mm outer diameter mounted on 600W Ryobi grinder. The technical characteristics of the cutting disc are defined by the code 41 99A 46 S7 BF given in the catalog. The first digit indicates the manufacturer symbol, 99A indicates that abrasive material is made of aluminium oxide, 46 is the medium hard grain size, S7 is hardness and BF is a kind of resin used for bonding. The abrasive material of cut off disc with coarse grain size and high hardness enables the fast cutting.

Thin abrasive cutting discs have been used in this research. The abrasive cutting action is performed by ultra-thin steel cutting disc of 1mm thickness; 22mm bore diameter and 115mm outer diameter mounted on 600W Ryobi grinder. The technical characteristics of the cutting disc are defined by the code 41 99A 46 S7 BF given in the catalog[58]. The first digit indicates the manufacturer symbol, 99A indicates that abrasive material is made of aluminium oxide, 46 is the medium hard grain size, S7 is hardness and BF is a kind of resin used for bonding. The abrasive material of cut off disc with coarse grain size and high hardness enables the fast cutting [59, 60]. Materials of S235JR, C45K, and ferrous aluminium based intermetallic alloy (Fe-Al40%) have been cut with standard steel cutting discs.

2.2 Measurement of experimental data

2.2.1 Electrical Energy Measurement

The electrical energy consumed during the process was measured with an analog power analyzer built with an AD633 chip-It provides the instantaneous product values of current and voltage. A channel recorder logger Velleman K8047 connected to a computer allows collecting the power signal with a sampling frequency of 0.01s.

Figure 8 shows the power curve for a cutting experiment on S235JR material with V_f at 1.488 mm/s. The behaviour observed in all the experiments is similar and can be divided into three stages. The first stage corresponds to the energy consumption when the disc is not cutting. The second stage is the transition stage in which cutting begins, characterized by a rapid increase in cutting power. Whereas, the third stage is the stabilization stage of power consumption. The average power consumed in this last stage E_e, is used to estimate the SEC. With the help of regression Eq. (6), P_m is obtained as a function of the measured E_e.

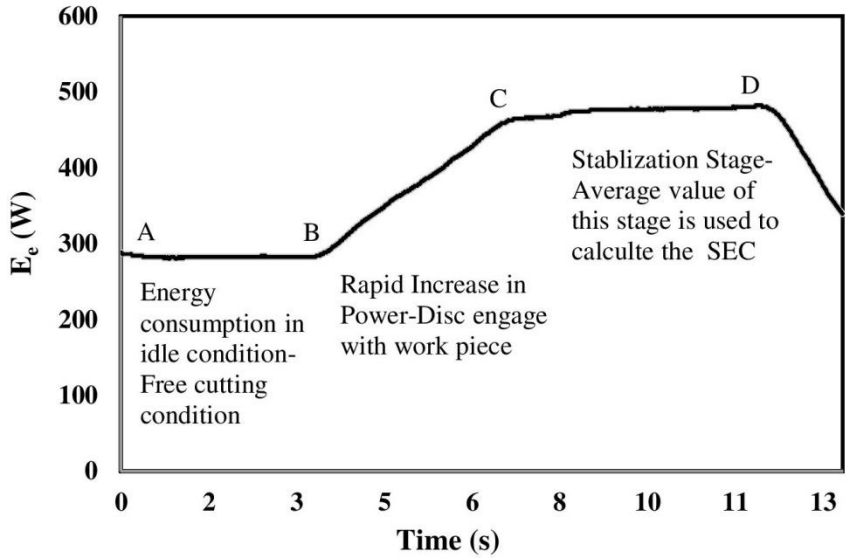

	T(s)	E_e(W)
A	0.0	288
B	3.3	382
C	6.9	469
D	11.7	480

Figure 8. Electrical Energy consumption behavior

2.2.2 Measurement of material removal rate

To measure the material removal rate in equation (5), a general model of material removal rate for this experiment has been used which is the product of feed rate and cutting cross section [16].

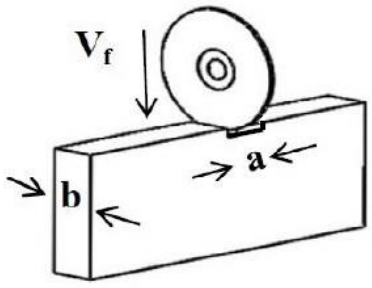

Figure 9. Cutting cross section

$$Q_w = A_c\, V_f \tag{7}$$

Feed rate V_f in Eq. (7) is a function of the rotation speed of the stepper motor. A kinematic study of the spatial movement of the centre point, where cutting disc is mounted, has been carried out using generalized coordinates [61]. The kinematic study showed that given a constant rotation speed of the stepper motor, the feed rate V_f at the cutting point is vertical and remained

constant throughout the cutting cross section. The feed rate values obtained from kinematic studies were verified by the time taken for the cutting discs to cut through the length of the workpiece.

The cutting cross section A_c shown in Eq.(7) is perpendicular to the feed rate, and is defined by the product of material thickness 'b' and width of cutting thickness 'a' as shown in figure 9. The widths of specimen are 3, 10 and 4.6 mm for S235JR, C45K and intermetallic Fe-Al (40%), respectively, and cutting thickness is 1.8 mm. The cutting thickness has found to be higher than the thickness of cutting disc. It was verified that the actual thickness of cutting did not coincide with the information provided by the manufacturer for 1mm thick cutting disc. It was also determined that there was an axial deviation of cutting disc, when it was rotated in free cutting condition. The feed rates used in this experiment are high for these kinds of discs. So, during material cutting, the further bending and vibration of cutting disc have increased the cutting thickness.

2.2.3 Measurement of cutting thickness

The cutting thickness of each specimen is measured with a WADEO iT33-MDUK digital microscope with a 2 Mega pixel image sensor. The measurement of thickness was calculated with Image J2 open source software for scientific image analysis, developed by the University of Wisconsin-Madison. The width of the specimen is measured with digital vernier-caliper. The equipment allowed selecting four different feed rates previously set at 0.539mm/s, 0.613mm/s, 0.899mm/s and 1.488 mm/s. As there is a probability that grains alignment may not be uniform in the work piece material and cutting disc, and small lateral vibration of cutting disc at lower feed rates, a small change in material removal rate was found for the same feed rate. To compensate for this, the cutting experiment is repeated 4 times for each feed rate.

2.2.4 Sliding Power measurement

Sliding power (P_{sl}) has been measured through a separate experiment and is explained through figure 10. Cutting disc is engaged with work piece material at the specific feed rate. When the cutting disc reached the middle of cutting path and power consumption is stabilized, the feed rate is stopped at point A, keeping the cutting disc in running condition. Stopping the feed rate produced the sudden drop in power, and it is again stabilized at point P. This operation kept the cutting disc in contact with the material without chip removal and without producing plastic deformation. The power measured at the intersection point P of regression lines BC and DE is only associated with the sliding phenomenon. The Sliding power measured in per unit of cutting area for all the materials is given in figure 1

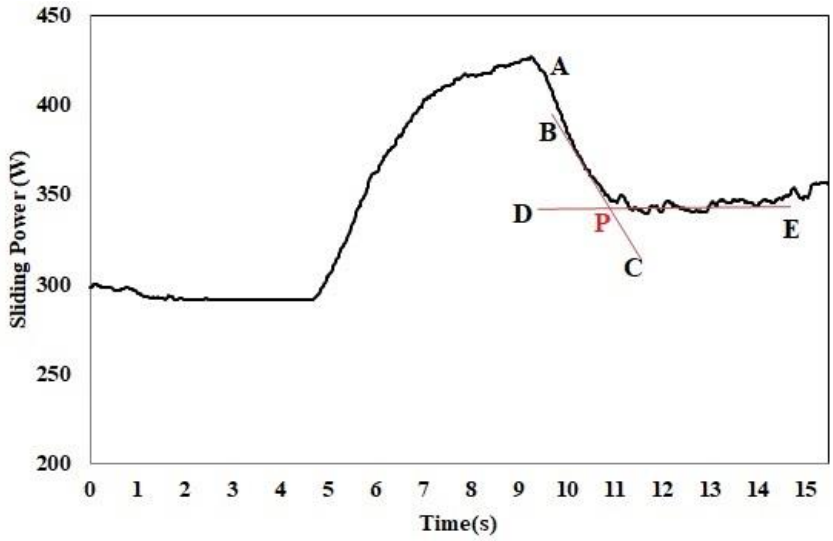

Figure 10. Sliding Power measurement for C45K-Q+T

2.3 Model of Specific Energy Consumption

The cutting model is based on the fact that mechanical power consumed by cutting (P_m) is equal to the summation of power consumed by sliding (P_{sl}), power consumed by plowing (P_{pl}) and power consumed by chip formation (P_{ch}).

$$P_m = P_{sl} + P_{pl} + P_{ch} \tag{8}$$

The relationship between specific cutting energy and material removal rate shown in figures.11 and 12 is estimated by the empirical model shown in Eq. 8.

$$\frac{P_m - P_{sl}}{Q_w} = \frac{P_{pl}}{Q_w} + SCE \tag{8}$$

Where SCE is the quotient of stock removal power (P_h) and the material removal rate (Q_w). This model presented in Eq. (8) was proposed by Gutowski et al.[62] and later validated by Kara and Li [63]on the basis of experimental results. The adopted model demonstrated the statistical accuracy to evaluate the specific energy consumption(SEC) with respect to material removal rate for the processes of grinding, milling, turning and injection moulding [64]. Recently, Napoles et al. [50] adopted the same model for surface grinding to analyse the three energy components during industrial scale surface grinding.

2.4 Results and discussions

It has been verified through the proposed model in Eq. (8), that the values of power dissipated by phenomenon of sliding (P_{sl}), plowing (P_{pl}) and specific cutting energy(SCE) are constants for a material as shown in table 3. These constant values of plowing (P_{pl}) and specific cutting energy (SCE) are coefficients of Eq. (8), and has been used to draw the experimental graphs in figures. 11 and 12. These coefficients are obtained by adjusting the experimental data by least squares. Figures 11 and 12 indicate that the behaviour of this model is asymptotic, with the increase in material removal rate, the ratio of P_{pl} to Q_w decreases and at very high material removal rate plowing energy reduces significantly. The reduction of plowing energy in terms of percentage has also been shown in figure 14. The reduction of plowing energy with material removal rate is in agreement with the previous research on grinding[31, 50]. Sliding power (P_{sl}) depends on the rotational speed of the cutting disc. In this particular experiment, the rotational speed of the cutting disc is constant and it undergoes for a very small change depending on the feed rate, so sliding power remains constant. The regression applied to the experimental data of materials has values of the coefficient of regression R^2 greater than or equal to 0.872. The coefficient of determination, close to unity for most of the materials, shows the good fit between equation (8) and the experimental data of SEC.

One way analysis of variance (ANOVA) single factor is applied to the mean specific energy values for the four feed rates as shown in table 4. The variations of mean values of specific energy consumption are statistically significant with p values of less than 0.05 for most of the materials. Therefore, the feed rates used to produce different energy consumption, do not belong to the same family of cutting conditions.

Materials	P_{sl}	P_{pl}	*SCE*	R^2
Units	J/s	J/s	J/mm^3	
S235JR	29.16	163.69	37.5	0.956
Intermetallic-FeAl40%	77.36	113.19	13.08	0.878
C45K-Q	99.36	228.04	7.82	0.912
C45K-Q+T	117.36	216.21	4.93	0.923
C45K	127.36	152.18	4.16	0.872

Table 3. Asymptotic Parameter Values and sliding power

In general, for all the materials, specific energy consumption (SEC) is decreasing asymptotically with the increase in material removal rate; which confirms the accuracy of the adopted methodology. It is evident from the graphs in figure11, and 12 that at a very small material removal rate, SEC is very high. This phenomenon known as the size affect [31]. With the increase in material removal rate, SEC decreased. This decrease in SEC is only due to the

decrease of plowing energy ($\frac{P_{pl}}{Q_w}$), as specific cutting energy (SCE) for material deformation has the constant value. So, at a higher stock removal rate, SEC reduces to a minimum value.

Source	SS	df	MS	F	P-value	F-critical
C45K	326.49	3	108.8	75.784	3.68E-05	4.757
C45K-Q+T	147.3	2	73.65	4.4783	0.06456	5.143
C45K-Q	343.13	2	171.6	26.736	0.001027	5.143
Fe-Al40%	941.94	3	314	24.823	0.000418	4.347
S235JR	80468	3	26823	57.243	9.49E-08	3.411

Table 4. Asymptotic Parameter Values and sliding power

This minimum energy is the specific cutting energy (*SCE*) energy and it has remained constant through the whole cutting process as confirmed by Malkin [31]. According to Shaw[52], in stock removal grinding process, most of the energy is dissipated as the shear cutting energy to produce the chips. However, he conducted the abrasive cutting off operation at very higher feed rates (5-60 ipm or 2.1-25.4 mm/s) [9]. The dominance of shear cutting energy in their experiments is attributed to the use of very high feed rates.

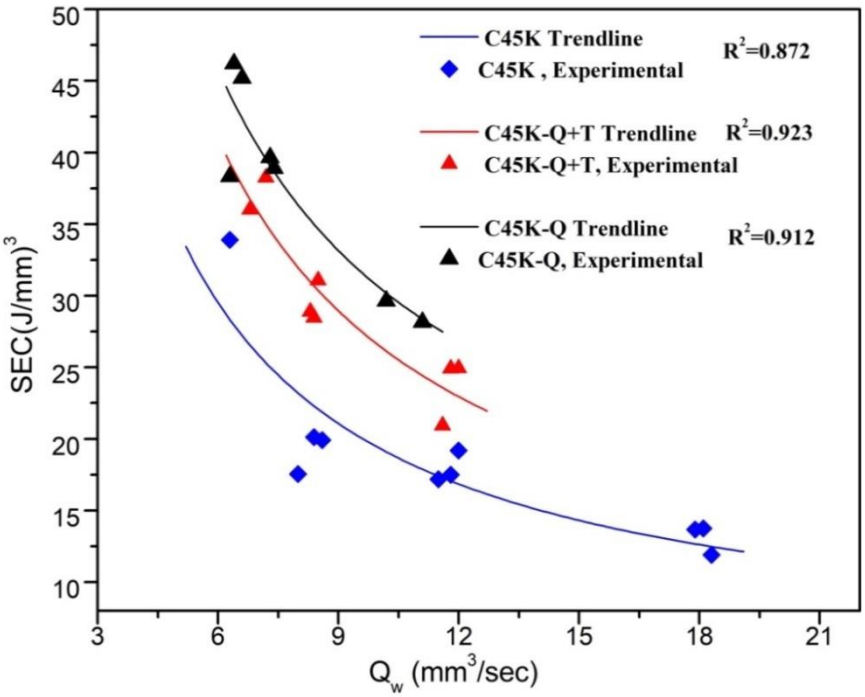

Figure 11 SEC relationship with material removal rate for C45K, C45K-Q+T, C45K-Q

The range of feed rates in this experiment (0.5- 1.488 mm/s) is low in comparison to the feed rates used by Shaw in his experiments. The given feed rate values are supported by the grinder used; higher values of feed rates than this range stopped the cutting machine. Lower values of feed rates allowed the cutting disc to sufficiently deform the material before breaking, which is the reason for dominance of plowing energy and low value of specific cutting energy (SCE).

Figure.11 is showing the SEC relationship with material removal rate for three materials of C45K normal and with different thermal treatments. C45K-Q has the highest specific energy consumption (SEC) with the highest value of hardness, followed by C45K-Q+T with the lowest value of hardness. C45K has the lowest specific energy consumption among three materials although its hardness is more than C45K-Q+T.The specific energy consumption of these three materials and its correlation with material hardness is exhibiting a different trend from the previous research conducted by Napoles et al. [50] on the same materials for surface grinding.

The thermal treatment made a significant impact on the behaviour of specific energy consumption (SEC) and specific cutting energy (*SCE*) of the materials. The SEC of C45K-Q steel is the highest among three specimens of C45K, because of large value of hardness. Marinescu et al.[65] evaluated that increase in hardness increases the resistance to abrasive machining, so cutting forces and machining difficulty increases. C45K tempered steel is consuming a higher value of specific energy as compared to C45K despite the low value of hardness. This is due to the reason that tempering is performed to reduce the hardness and increase the toughness and ductility of material [66]. Increase in toughness increases the energy required to deform the material [67]. The three materials are showing the same trend of decrease in specific energy consumption (SEC).

However, for quenched and tempered steel, at large material removal rate, the machine did not give an accurate representation of the energy consumed and cutting disc got jammed into the work piece. This indicates that thermal treatment has a considerable effect on the machinability of the materials. It also showed that this cutting disc has limitation for specific materials under certain cutting conditions. Thermal treatment of C45K also affected the specific cutting energy (*SCE*). As seen from table 3, C45K, C45K-Q+T and C45Q have considerable differences in values of specific cutting energy. However, according to Malkin and Joseph [48] minimum energy required to produce chips in abrasive process is not affected by little alloying or heat treatment. So the difference of specific cutting energy (*SCE*) due to heat treatment of C45K in this experiment is not in agreement with Malkin and Joseph's finding.

Among the metallic alloys, S235 JR with the lowest hardness has the highest SEC and *SCE* as shown in figure 12a. The carbon content of S235JR is comparatively lower among specimens, low carbon steel is more ductile so more energy is required to machine the low carbon steel as compared to the medium carbon steel and are comparatively difficult to machine [68].

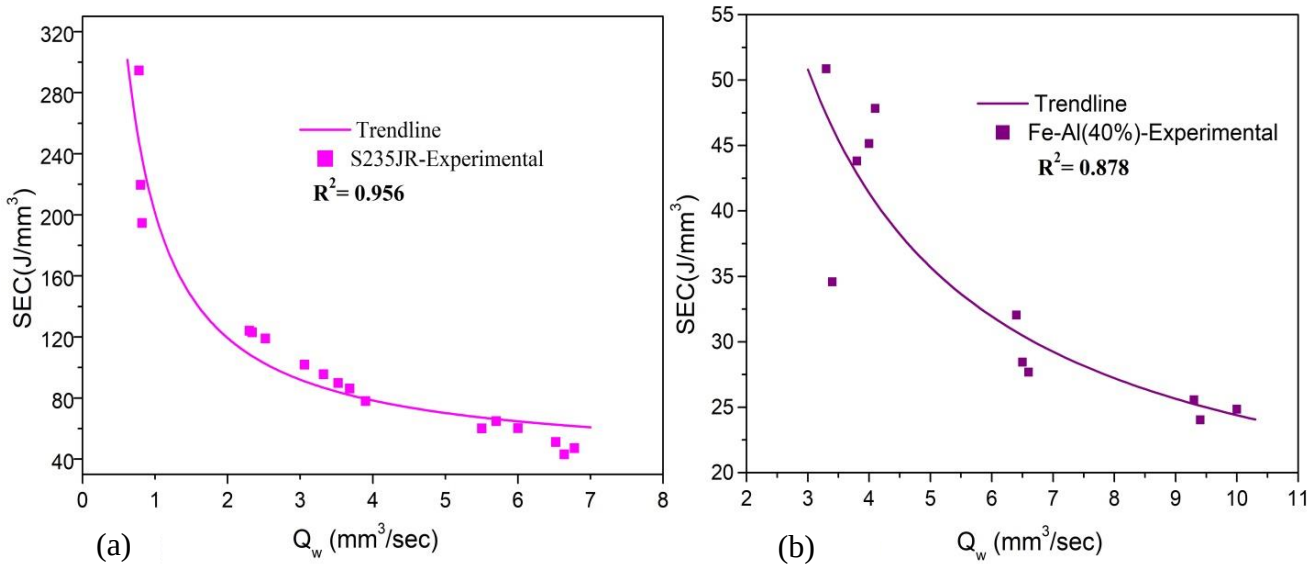

Figure 12 SEC relationship with material removal rate for (a) S235JR and (b) Intermetallic Fe-Al(40%)

In comparison to brittle materials, ductile materials undergo extensive plastic deformation before fracture [69]. Huge amount of plastic deformation in ductile materials requires high value of specific energy to fracture the material [70, 71]. So, high value of SEC and *SCE* for S235JR is attributed to large plastic deformation due to high ductility.

The specific energy consumption (SEC) behaviour of intermetallic Fe-Al(40%) is shown in figure 12b. The value of hardness inter metallic Fe-Al(40%) is same as C45K and its specific energy consumption relationship with material removal follows the same trend as C45K normal. C45K is brittle due to higher carbon content. The same trend of expansion is attributed due to brittle nature of intermetallic Fe-Al (40%). Brittle fracture of inter metallic is due to weak grain boundaries and the higher concentration of the aluminium which limits the ductility of the material [57, 72, 73]. However, specific energy consumption of intermetallic Fe-Al (40%) is higher in comparison to C45K normal and with thermal treatment. As shown in table 3, the specific cutting energy (SCE) of intermetallic Fe-Al (40%) in percentage of total energy is higher in comparison to C45K normal and with thermal treatment. This indicates the comparatively little higher ductility of intermetallic Fe-Al(40%), which is the reason for high specific cutting energy. Saigal et al.[74] also reported the higher cutting forces for iron aluminides in comparison to medium carbon steel for milling operation.

2.4.1 Comparison of Sliding Energy

Figure.13 shows the comparison of sliding power per unit cutting area for all materials. The experiment in figure 10 revealed that sliding energy does not participate in material removal process; it is merely a rubbing or friction energy. For this reason, sliding power per unit of cutting area has been used. Sliding energy as the constant energy of friction has also been reported by Zhang et al. [75] and Barbara et al.[76].

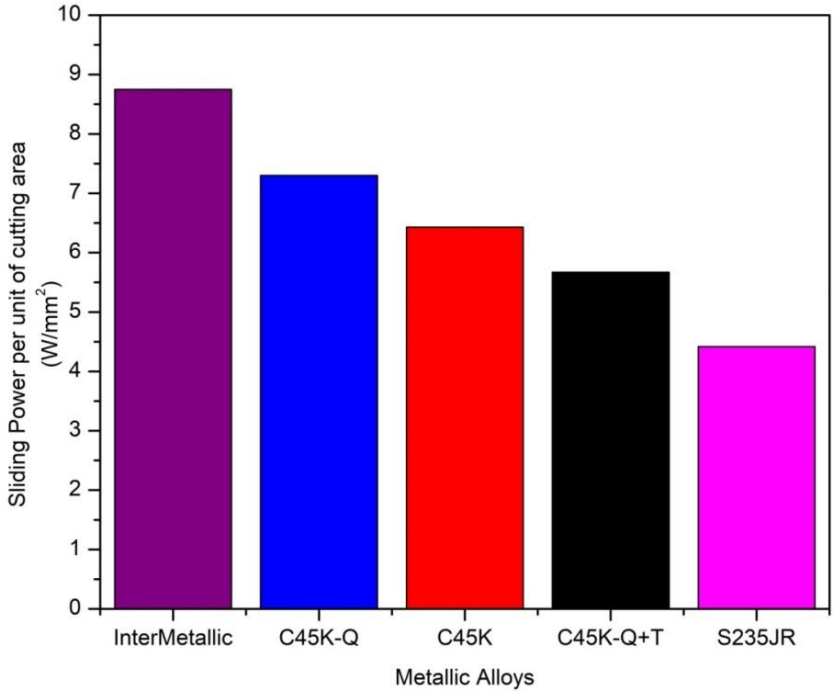

Figure 13 Comparison of Sliding Power per unit of cutting area for all materials

The highest value of sliding power per unit cutting area for intermetallic Fe-Al (40%) is due to its brittle nature at normal temperature. Sliding or rubbing power is dissipated during the initial contact of cutting grain with material, and it does not produce the material deformation. Brittle materials do not undergo any plastic deformation before fracture[16], so high sliding power for intermetallic Fe-Al(40%) is due to the reason that initial rubbing energy is absorbed by material without producing plastic deformation. Wu et al.[77] presented a model, which also provides some support to this argument, which states that in grinding of brittle materials, the main forms of energy dissipation are rubbing and chipping. S235JR has the highest ductility among the given materials, and ductile materials have the tendency to go under huge plastic deformation before fracture[69]. So plastic deformation for S235JR starts very earlier, and this is the reason for very low sliding power dissipation per unit cutting area. C45K family has the lower ductility in comparison to S235JR because of higher carbon content, which is the reason for comparatively higher sliding energy per unit of cutting area. Within C45K family, C45K-Q

has the highest hardness, which increases the brittleness and so sliding power per unit of cutting area increased. C45K-Q+T has less sliding power per unit cutting area in comparison to C45K because of thermal treatment. As tempering reduces hardness and increases the ductility of material, so sliding power per unit cutting area reduces.

2.4.2 Percentage contribution of specific energies in material removal

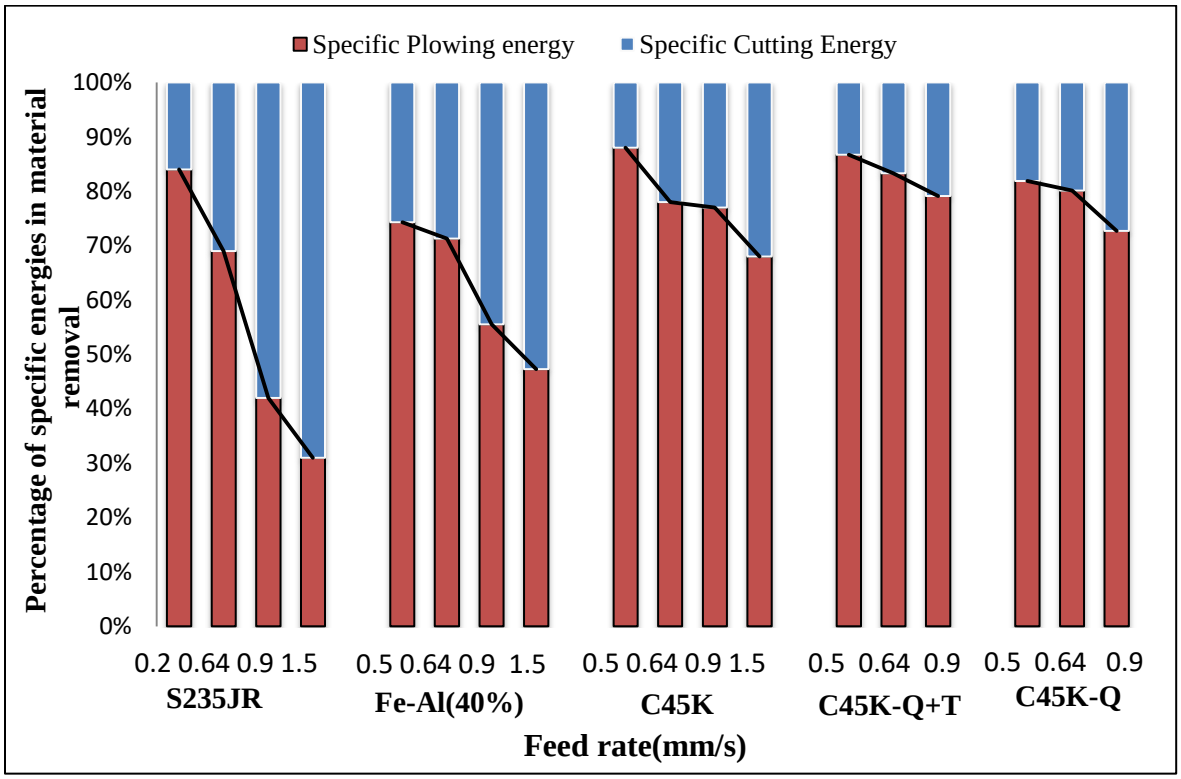

Figure 14 Percentage contribution of specific energies at different feed rates

To determine the percentage contribution of specific energy components for material removal, bar chart has been drawn as shown in figure 14. Sliding energy has not been shown in this graph, because it merely rubs and does not deform the material. For all materials, in general, specific plowing energy has been found to be the most significant phenomenon of total specific energy consumption. The dominance of plowing energy for these materials is due to the use of a comparatively low range of feed rates for this experiment. The contribution of plowing energy in terms of percentage is higher for C45 K family of materials, because of their high value of hardness. Even at high feed rates, plowing energy remained the most dominant phenomenon with 68%, 79% and 73% for C45K, C45K-Q+T and C45K-Q respectively. The dominance of plowing energy for hard and high strength materials has also been determined for grinding[38, 43]. The contribution of specific cutting energy (SCE) in terms of percentage is comparatively

higher for S235JR at higher feed rates. Due to the low value of hardness of S235JR, the transition from elastic to plastic deformation becomes easier at higher feed rates, which rapidly reduced the plowing energy.

2.5 Cutting Power relationship with feed rate

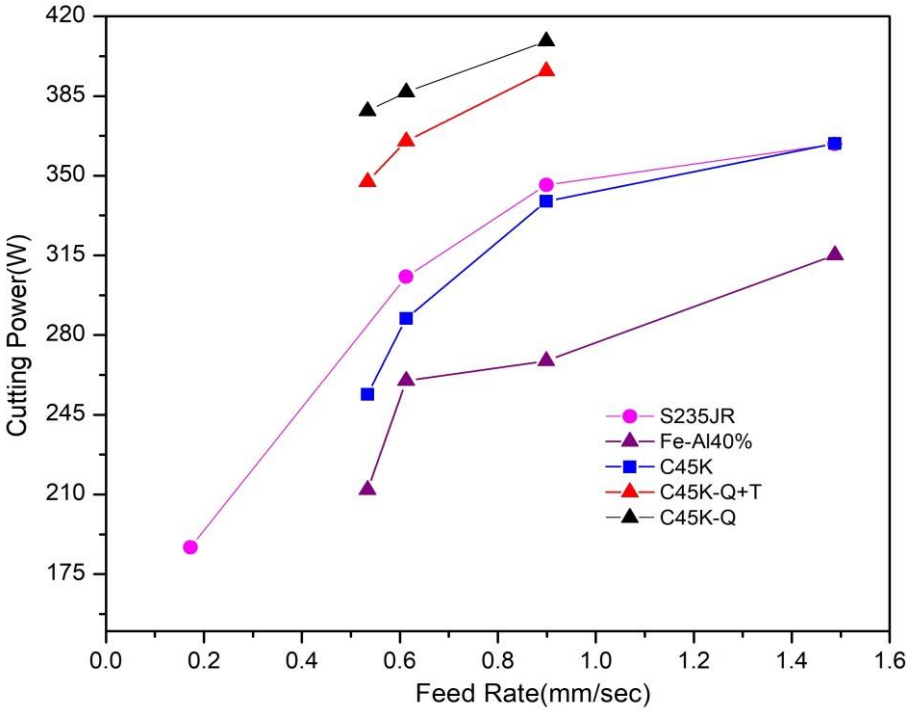

Figure 15 Cutting Power relationship with feed rate for C45K, C45K-Q+T, C45Q, S235JR and Intermetallic-FeAl40%

The cutting power depends on material properties and feed rate. The relationship of cutting power with feed rate for C45K and S235JR is shown in figure 15. It indicates that cutting power increases with increase in feed rate, however at a certain higher feed rate, the increase in cutting power reduces and the curve tends to flat. At high feed rates, cutting grains become sharper and consume less power for metal cutting and hence cutting force decreases. This behaviour is analogous to the research finding of Shaw in his study for abrasive cut off operation [9]. Cutting power relationship with feed rate for intermetallic Fe-Al (40%) did not follow the general trend. As seen in figure 15, cutting power for Fe-Al (40%) at a high feed rate did not lower and increased to a higher value. This increase in cutting power is attributed to an increase in ductility of material due to high temperature encountered at high feed rates. At high feed rates, an increase in temperature increases the yield stress, hence, the ductility of intermetallic Fe-Al(40%) increases [78, 79]. An increase in ductility also increased the power to cut the material.

2.6 Conclusion

An experimental set up has been successfully designed, and manufactured to perform the abrasive cut off operation using commercial standard grinder and standard cutting discs. The adopted experimental technique made use of conventional power measurement through dynamometer to devise a new way of measuring the specific energy consumption. Making use of regression equation to find the mechanical power by just measuring the electrical energy during abrasive cutting, simplified the experimental procedure. The specific energy consumption (SEC) was then characterized and analysed with the change in material removal rate. It has been found that abrasive cutting with this experimental set up is suitable for comparatively brittle materials at low and medium feed rates. The Specific cutting energy (SCE) is the minimum amount of energy required to deform the material, and at very higher feed rates it is the only apparent form of energy, as plowing energy becomes negligible.

Material properties and thermal treatment have a significant influence on specific energy consumption (SEC) and specific cutting energy (SCE). Steel with low carbon content consumed a high value of specific energy consumption, because of high ductility. As the carbon content of steel is increased, material brittleness is also increased, which decreased the specific energy consumption (SEC). In case of C45 steel, it has been found that quenching of material increased the SEC and SCE while tempering after quenching decreased the specific cutting energy (SCE) and SEC. Sliding power per unit of cutting area is higher for brittle materials and lower for materials with comparatively higher ductility. Plowing energy was the most prominent phenomenon of energy dissipation for all the materials. At higher feed rates, the major dominance of specific cutting energy (SCE) in terms of percentage of total material removal energy, was observed for S235JR, and intermetallic Fe-Al(40%) at 69% and 53% respectively. For C45K family of materials, even at higher feed rates, plowing energy remained the most significant phenomenon.

Chapter 3

Modelling of specific energy consumption in to components

The model of specific energy consumption presented in chapter 3 characterizes the specific energy consumption in to components of sliding, plowing and specific cutting energy. However, the detailed models of specific energy components, which comprehensively explained their relationship and sensitivity with process parameters was a gap. This chapter aims to put forth the modelling of specific energy consumption on the basis of the comprehensive models of primary and secondary rubbing energies, specific plowing energy and specific cutting energy. The model development, takes in to account the triangular shape of semi super abrasive cubitron grits. The model has been validated through experimental data, using the same methodology devised in chapter 2. This model will help to better understand the influence of process parameters, cutting conditions, and mechanical properties of the materials on specific energy consumption and its components.

Using cubitron cutting disc, the abrasive cut off operation has been performed on the materials Al 7075, Al 1100, oxygen free copper OFC(C10100), Inconel 718 and SS201. The cutting action of abrasive disc is shown in figure 16a, where feed rate V_f is defined by the function of stepper motor operating the mechanism[80].

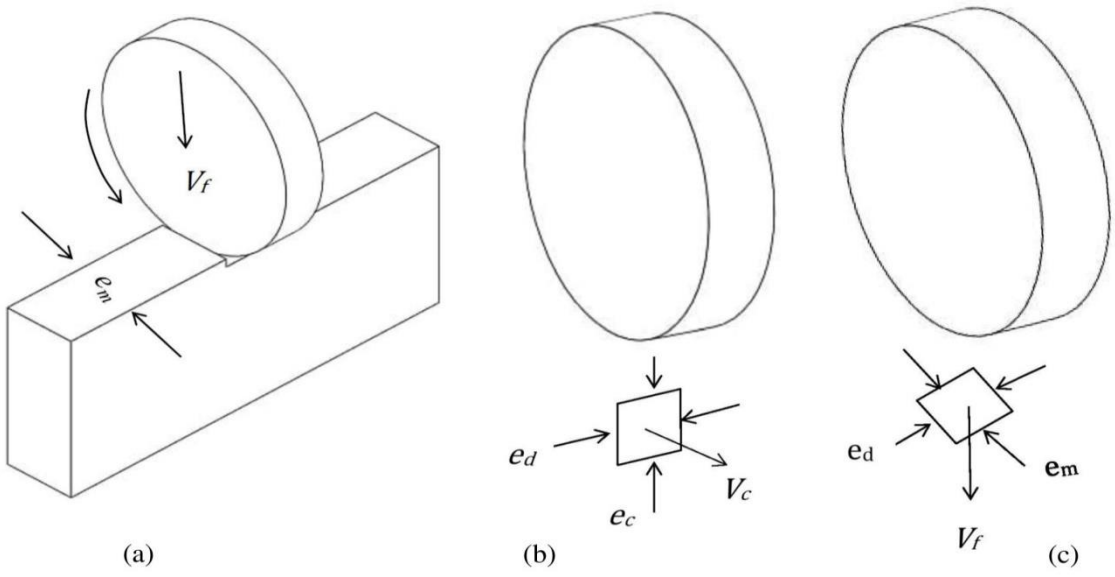

Figure 16 (a) Metal cutting with abrasive disc and material removal rate with (b) feed velocity and (c) cutting velocity

The product of the feed rate and the cutting section A_c determines the material removal rate as seen figure 16c.

3.1 Individual models of specific energy components

3.1.1 Ploughing Energy Model

The assumption that the entire volume traversed by the abrasive grain is removed by the abrasive wear mechanism is not correct [81]. In ductile metals part of the material accumulates at the edges of the groove defined by the abrasive as shown in figure 17.

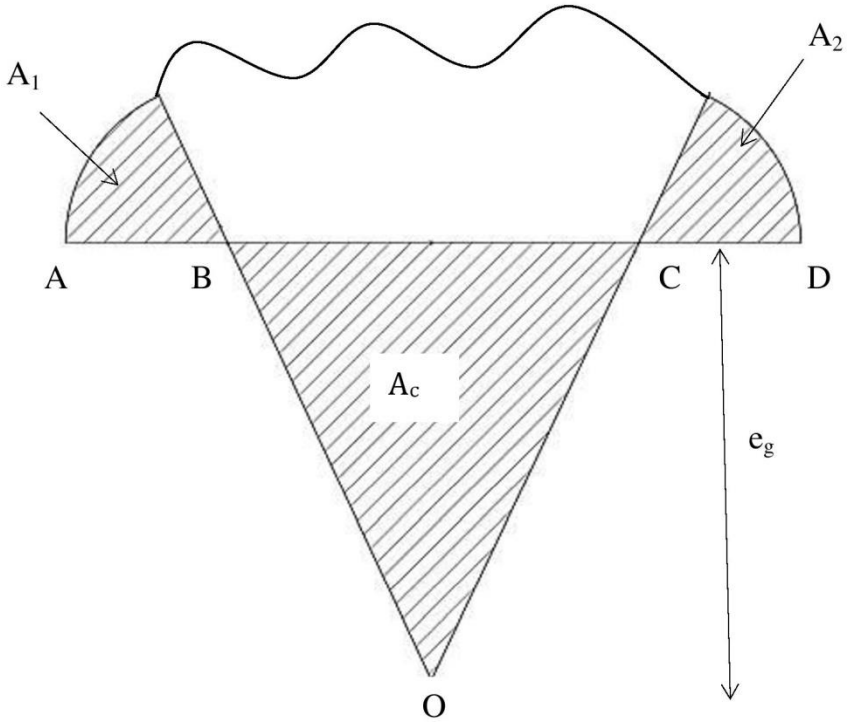

Figure 17. Abrasion and build up on ductile material

The f_{ab} factor is introduced to define the ratio between the volume of material removed from the surface and the volume of the groove formed by the movement of the abrasive.

$$f_{ab} = 1 - \frac{(A_1 + A_2)}{A} \tag{9}$$

where (A_1+A_2) is the cross-sectional area of material accumulated around the edges of the groove, A is the cross-sectional area of material defined by the movement of the abrasive, f_{ab} is a dimensionless parameter defined in the range (0-1)[82].

If f_{ab} is equal to zero, all the material in the groove formed by the movement of the abrasive grain is stacked. In this case there is no chip formation. If f_{ab} is equal to 1, all the material in the groove formed by the movement of the abrasive grain is removed from the work piece. This would be the case of an ideal cutting.The rate of material removed per grit Q_g is defined as

$$Q_g = f_{ab} * A * V_c \tag{10}$$

where V_c is the cutting speed defined by the peripheral speed of the disc. A is a function of the square of the depth of cut e_g of a pyramidal grit multiplied by a constant C_1 which depends on the angle defining the pyramid.

The rate of material removed by all the grits is a function of the grit number N and the equivalent depth of cut e_c , among other parameters and constants [5]. The rate of material removed by a cut-off wheel during the plowing can be defined as

$$Q_{pl} = N \cdot f_{ab} \cdot {e_c}^2 C_1 \cdot V_c \tag{11}$$

The Specific Energy Consumed with ploughing is defined as

$$SEC_{pl} = \frac{C_{pl}}{{e_c}^2 \cdot V_c} \tag{12}$$

where C_{pl} is a constant function of the number of active grit, the shape of the grit and the f_{ab} factor.

In figure 16, the rate of material removed from a cut-off wheel as a function of cutting speed V_c and velocity rate V_f is shown. For a disc diameter much larger than the material thickness, the cutting path of grit is a straight line of length the material thickness e_m. And the material removal rate can be defined as the product of the cutting speed V_c by the square section ($e_c \cdot e_d$), as shown in figure 1b. Similarly the material removal rate can be defined as the product of the velocity rate V_f by the square section ($e_d \cdot e_m$), as shown in figure 16c. Both removal rates characterise the same volume of material removed per unit time. Making both expressions equal gives the equivalent depth of cut

$$e_c = \frac{V_f}{V_c} e_m \tag{13}$$

Replacing (13) in (12) and assuming that the rate of material removed is defined as in figure 16c

$$SEC_{pl} = \frac{C_{pl} V_c {e_d}^2}{Q_w^2} \tag{14}$$

As the thickness of the cutting disc e_d and C_{pl} are constants, specific plowing energy is the function of cutting velocity and material removal rate. The specific plowing energy is more sensitive to material removal rate in comparison to cutting velocity.

3.1.2 Primary rubbing energy

The primary rubbing energy is the phenomena of rubbing of grit tip against the work piece surface without penetration [82]. This energy does not contribute to material removal and is one of the main reasons for the high specific energy consumed during the grinding. Vijayender defined the primary friction energy as the energy dissipated by the grit contact with the material surface without penetration [38]. The grit shape has an edge radius which rubs against the material surface due to the structural rigidity of the machine, producing a primary frictional force.

The Specific Energy Consumed with primary rubbing is defined as

$$SEC_{pr} = \frac{C_{pr} V_c}{Q_w} \tag{15}$$

Where C_{pr} is the coefficient of primary rubbing energy. This constant is a function of the friction force and the number of active grains

3.1.3 Secondary rubbing energy

Secondary rubbing occurs between the cutting edge and the workpiece mainly due to high (negative) grit angles of the abrasive grits [38]. Secondary friction occurs mainly along the entire length of the scratch, produced by the abrasive grit along the BOC as shown in figure 17. As the ploughed material is not so stiff, the friction between the surfaces AB and CD is assumed to be negligible. Specific Energy Consumed with secondary rubbing is defined as

$$SEC_{sr} = \frac{C_{sr} \cdot V_c}{Q_w} \tag{16}$$

Where C_{sr} is a constant resulting from the product of the average value of the tangential shear force for a grain by the number of active grit rubbing against the surface of the material.

3.1.4 Specific cutting energy

Malkin [31] believes that the energy required to form a chip is equal to the adiabatic melting energy of the work material. It is known that the melting phenomenon does not occur in grinding or cutting processes with abrasive discs. The time scale of chip formation as indicated above indirectly supports the hypothesis of Malkin. Malkin's hypothesis defines the specific cutting energy as a property of the material, where the SCE does not depend on the cutting conditions of the process and can therefore be assumed as a constant in this model.

$$SCE = \frac{P_c}{Q_w} \tag{17}$$

Where P_c is the power of chip formation

3.2 Energy Conservation in cutting through abrasive disc

Applying the principle of energy conservation, the energy consumed per unit time during the metal cutting with abrasive discs is the sum of the energies consumed by each of the above mentioned mechanisms, sliding, ploughing and chip formation.

$$SEC = SEC_{pl} + SEC_{pr} + SEC_{sr} + SCE \tag{18}$$

Replacing (17), (16), (15) and (14) in (18) gives the energy conservation model for cutting with abrasive discs.

$$\frac{P_M}{Q_w} = \frac{C_p V_c {e_d}^2}{Q_w^2} + \frac{C_{sl} V_c}{Q_w} + SCE \tag{19}$$

Where $C_{sl} = C_{pr} + C_{sr}$

Material	C_{pl}	C_{sl}	SCE	R^2	Hardness (Brinell)
Al 7075	7.5E-18	0.0011	17.38	0.970	150
Al 1100	7.5E-03	0.0016	18.59	0.952	32
OFC-C10100	6.4E-18	0.0076	8.67	0.969	95
Inconel-718	3.4E-19	0.0025	22.92	0.998	340
SS201	1.5E-03	0.0009	20.82	0.957	121

Table 5. Coefficients of Model and materials hardness

The model constants, right-hand side of Eq. (19) shown in table 5, are obtained by performing a least squares regression of metal cutting experiments through thin abrasive discs. These experiments consist of measuring the mechanical power (P_m) consumed during the metal cutting, for different values of material removal rate as discussed in chapter 2. The hardness of the materials along with model coefficients are shown in table 5.

3.3 Results and Discussion

The behavior of the model Eq.(19) as depicted by the relationship of SEC with material removal rate, is asymptotic. As shown in figure 18, that with increase in material removal rate, specific energy consumption decreases, a trend which is similar to previous research in grinding[38, 50, 77, 83].

The concept of ductility helps to understand the overall energy consumption for materials. In ductile materials, the gumminess of work piece materials due to heat generation, and higher fracture toughness in comparison to brittle materials increases the machining difficulty and consequently more specific energy is required during metal cutting[84]. For this reason, the specific energy consumption of ductile materials like OFC-C10100 and Al-1100 is higher in comparison to other materials at the same material removal rate. In grinding of hard and less ductile materials, the crack growth rate during cutting with abrasive grits is higher, which reduces the energy required to deform the material[85]. For this reason, hard and less ductile materials of Inconel 718, SS201 and Al 7075, are comparatively consuming less specific energy.

Among these materials, Inconel-718 is consuming higher specific energy. This is due to its high value of hardness, higher strength, and higher resistance to cutting[86]. Increase in hardness, increases the resistance to penetration of the abrasive grain, so grinding energy increases[65]. However, in comparison to the difference in hardness of Inconel-718 with other hard materials, the difference in specific energy consumption is not that much higher.

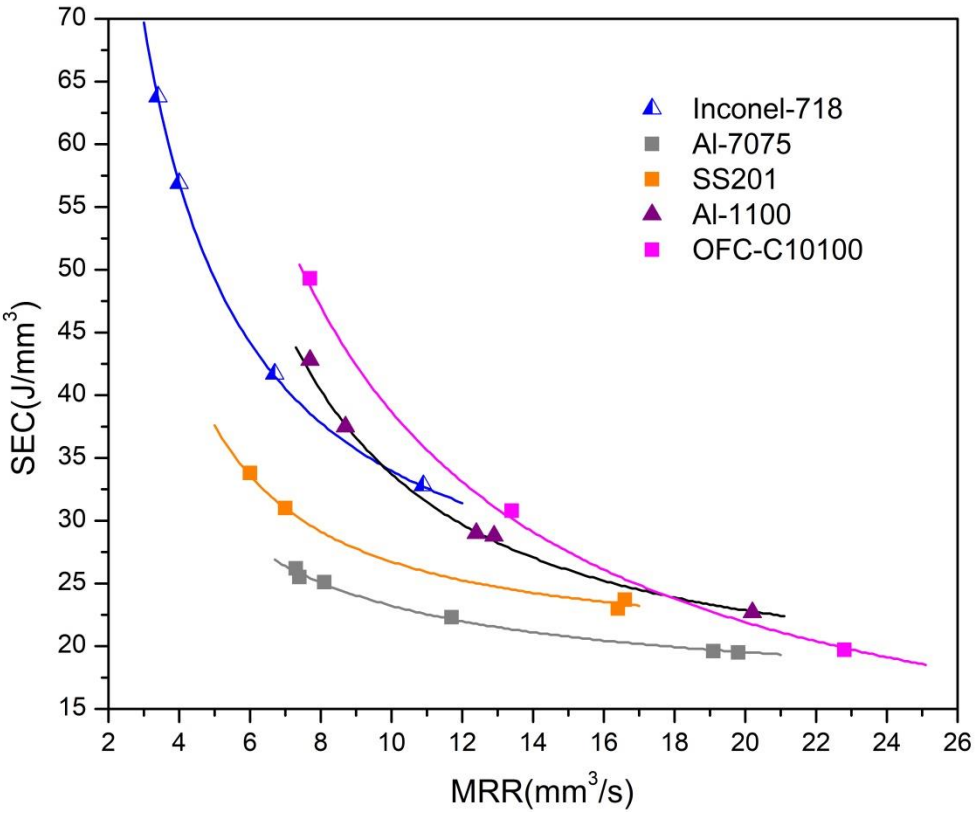

Figure 18 SEC relationship with material removal rate for all materials

This is due to the high suitability of cubitron wheels for grinding of Inconel-718, which reduce the abrasive resistance of the material, and can remain inert to higher cutting temperatures due to higher strength of the Inconel-718 [86, 87]. For Al-7075, the specific energy consumption is lowest and trend line is almost close to straight, which is an indication of major dominance of SCE at low and high material removal rate. Abachi et al.[88]attributed the low resistance to fracture due to fast crack initiation and crack propagation with in the microstructure.

Figure 19 shows the change in contribution of specific energy components with increase in material removal rate. It also reveals the influence of using cubitron on specific energy components. It is quite evident that SCE is the most dominant form of energy dissipation for most of the cases. It can be seen in figure19b that there is no plowing in materials of Al 7075, Inconel 718, and OFC-C10100 for the range of material removal used in this experiment. The dominance of SCE and absence of plowing energy in some materials is attributed, to the efficient cubitron grits. Cubitron are semi super abrasives, with precision shaped triangular grains which enable fast cutting[89]. According to Malkin [31], it is the possibility that plowing energy might not appear during grinding with super abrasives. He attributed the possibility of absence of plowing energy to the precision pyramidal shape of abrasive grains. The cutting points are much sharper and pointed, and at the faster cutting speeds, the transition from plowing to cutting phase is fast, which reduces the plowing force. Owing to fast and précised cutting ability of abrasive grain, SCE has found to be the most dominant form of energy consumption in most of the material.

Moreover, the model Eq. (19) also provides indication that specific plowing energy is more sensitive to material removal rate in comparison to sliding energy. It is changing inversely with square of material removal rate. It means, a small change in material removal can brings a significant change in specific plowing energy. At very low material removal rate, the appearance of plowing phenomenon could be possible. So, it might be possible that for these materials, there is a plowing phenomenon below the defined range of material removal rate used in this experiment.

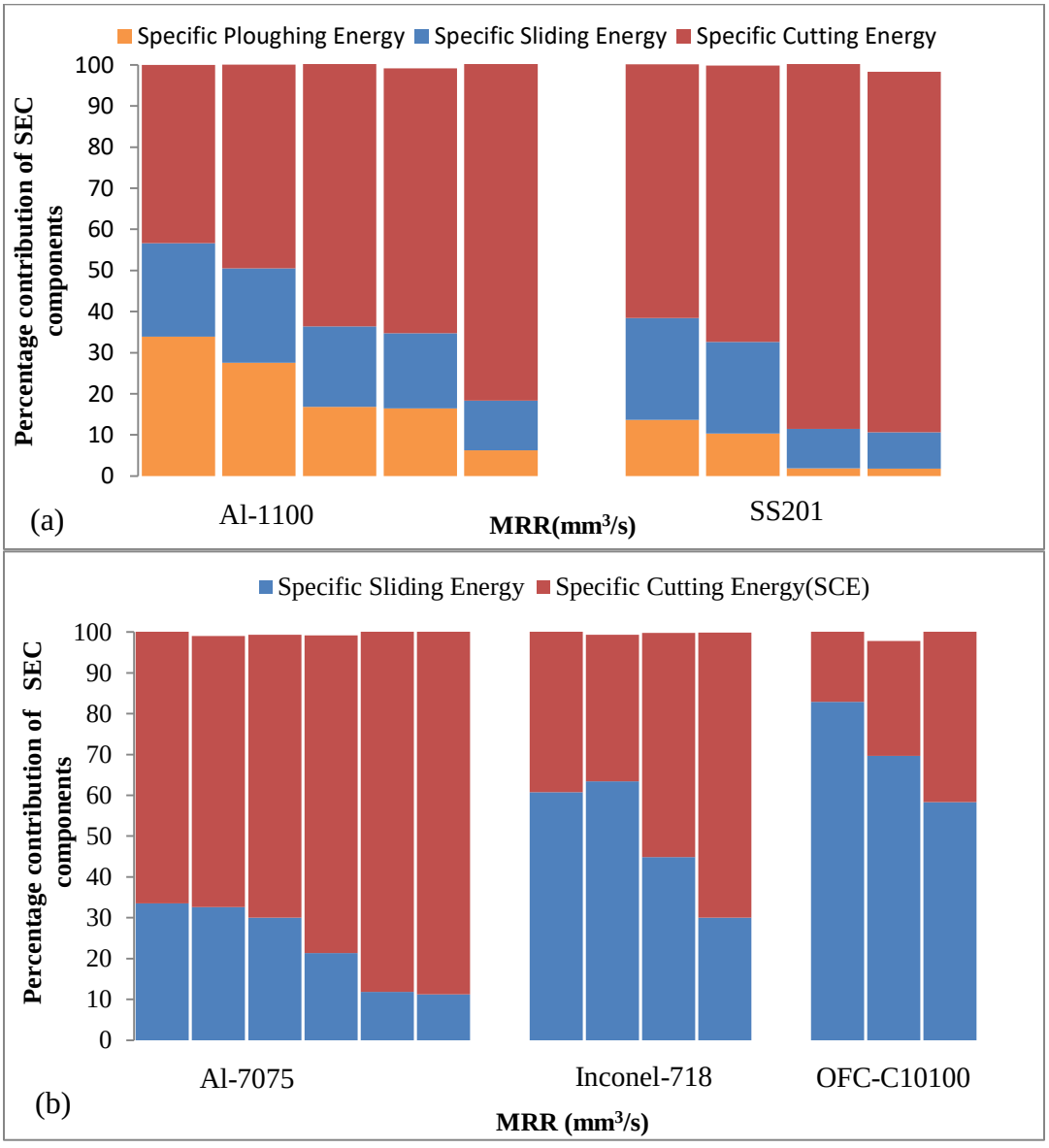

Figure 19 Contribution of sliding, plowing and SCE in material removal (a) Al-1100, SS201 (b) Al-7075, Inconel-718, OFC-C10100

During abrasive cut off operation, material properties played an important role in defining the dominance, presence and insignificance of specific energy components. For instance, Al 1100, and OFC-C10100, being both ductile materials have shown different behavior in this experiment.

The energy consumption in copper is dominated by sliding phenomenon. The apparent reason could be the high elasticity of Cu, in comparison to Al 1100[90, 91]. As sliding phenomenon takes place in the elastic regime of material deformation, so high value of elasticity indicates more resistance to rubbing, and increase the sliding energy. The absence of plowing phenomenon in OFC-C10100 is due to the grain refinement and dynamic recrystallization generation during the cutting process, which cause the fracture transformation from ductile to brittle[92]. So, after the elastic deformation, as the material entered in to the plastic state, the transformation to brittle nature, along with cutting action of sharper and pointed abrasive grits might have made the crack growth so fast that eliminated the plowing energy and also reduced the SCE. The lower SCE in brittle state is well in agreement with the previous research on abrasive cut off operation [77].

On the other hand, Al 1100 has low hardness, and failure is characterized by large strain deformation[93, 94]. For this reason, even with pointed and sharp cutting grains, the transition from elastic to plastic deformation takes time, and plowing is significant at low material removal rates. The high SCE of Al 1100 is attributed to increase in temperature in plastic deformation zone, which reduced the hardness and increased the ductility of the material, so energy required to produce chips increased[95].

Although SS201is hard material, but some plowing still appears at low material removal rate. The appearance of plowing is attributed to the very low material removal rate in SS201. The metal bar thickness of SS 201 is 5mm in comparison to other materials which ranged from 9-11mm. As a result, the material removal rate is comparatively low. As formulated in the model Eq. (19), plowing is very sensitive to material removal rate, so at a small material removal rate, plowing energy appeared in SS 201 as shown in figure 4b. The careful observation also reveals that small increases in material removal rate, the decreases or disappearance of plowing energy is also fast, in comparison to sliding energy. This proves the validation of model Eq. (19).

The absence of plowing in inconel-718 is not in agreement with the previous research on grinding. Plowing appears to be a significant phenomenon in experimentation conducted by Sinha et al. [43] during surface grinding of Inconel-718. Similarly Tahsin et. al's [96] study during single grit grinding of Inconel-718, also revealed the prominent plowing phenomenon. However, in these studies, depth of cut and in feed rates is low, which is the reason for prominent plowing energy phenomenon. The high SCE and SEC values in Inconel-718 could also be due to the work hardening of the material during the grinding process[97].

3.4 Discussion on Malkin's hypothesis about SCE and adiabatic melting energy

Malkin opined that specific chip formation energy (SCE) is roughly equal to the specific melting energy for wide range of materials, and plastic deformation energy should not exceed the adiabatic melting energy[98, 99]. However, melting does not occur in grinding. He further stated 75% of specific chip formation energy is actually shearing energy and remaining 25% of energy is expended in the friction between chip and tool[31]. Table 6 shows that only few materials are in agreement with the Makin's hypothesis. Cu and medium carbon steel C45K with thermal treatments, somehow followed Malkin's hypothesis. The difference of SCE and adiabatic melting energy for these materials can be attributed to the friction between grit and chip. Similarly, Ghosh et al[100] found 40% difference between specific chip formation energy and adiabatic melting energy during grinding of AISI 52100 bearing steel. They attributed the difference in energy to the friction between abrasive grit and chip.

On the basis of experimental results, it can be stated that oxygen free copper OFC-C10100 and medium carbon steels show good agreement to the Makin's hypothesis. For steels, apart from grit chip friction, there could be other factors that contribute to the difference in SCE and adiabatic melting energy. The parameters to calculate the adiabatic melting energy have been taken from various sources, and are standard values of the materials.

Materials	**C_p(J/kg.K)**	**ρ (kg/m^3)**	**Melting Temp (K)**	**L ρ (J/mm^3)**	**$U_{adiabatic} = \rho \int_o^T C_p dt + L\rho$**	**SCE (J/mm^3)**	**SCE-$U_{adiabatic}$**
OFC-C10100	390	8940	1356	1.84	6.57	8.7	24%
C45K-Q	480	7870	1720	1.97	8.46	12.3	31%
C45K	480	7870	1720	1.97	8.46	12.3	31%
C45K-Q+T	480	7870	1720	1.97	8.46	16.1	47%
SS201	500	7860	1783	2.20	9.21	20.2	54%
S235JR	460	7800	1773	1.95	8.36	25.0	67%
Inconel-718	440	8497	1698	1.86	8.21	22.9	64%
Al-7075	960	2800	873	1.11	3.46	17.4	80%
Al-1100	904	2720	913	1.08	3.32	18.6	82%

Table 6. SCE and Adiabatic melting energy

They do not correspond exactly to the materials which have been used in this experiment, so there is a probability of little deviation of adiabatic melting energy for this particular experiment. The difference of SCE and adiabatic melting energy for other materials is significantly higher and this difference cannot be attributed to grit chip friction. This could be drawback of Malkin's hypothesis; it is true for few materials under specific grinding conditions and cannot be generally applied.

3.5 Conclusion

In this study, the detailed models of primary and secondary rubbing energies, specific plowing energy and specific cutting energy are developed and validated through experimental data. The developed model enabled to understand the contribution of sliding, plowing and SCE with change in material removal rate during abrasive cut off operation. It was found out that grit shape has notable affect on material removal mechanism and the corresponding specific energy consumption. The model development and validation revealed that due to sharp, and pointed triangular abrasive grits, plowing energy turned out to be more sensitive to material removal rate than sliding. It changes inversely with square of material removal rate, due to sharpness of cubitron grits. For the material removal range used in this experiment, plowing energy did not appear for the materials of Cu, Al 7075, and Inconel 718. The brittle fracture in these materials, combined with fast cutting of sharp triangular grits made the transition from sliding to specific cutting energy very fast that plowing energy could not appear. In SS 201, plowing appeared due to low material removal rate resulted from small thickness of the material used. Due to high efficiency of cubitron grits, SCE remained the most dominant specific energy components in most of the materials. Cutting with cubitron discs minimized the redundant energies of sliding and plowing. With the developed model and cutting conditions, SCE of for all the materials has been found to be higher than their adiabatic melting energy. Malkin's hypothesis is applicable for copper and medium carbon steels, as the difference between SCE and adiabatic melting energy in these materials can be attributed to the friction energy carried away by the chips.

Chapter 4
Model of material removal by single cutting grain, equivalent chip thickness and upper bound analysis

Previous chapters focus on the energy dissipation of grain work piece interaction during different stages of material removal mechanism. The aim of this chapter is to study the material deformation through the trajectory of the single cutting grain at the micro scale. Applying the upper bound theorem on the orthogonal cutting model, distribution of shear strain rate at the primary deformation zone has been discussed. It is theoretical chapter, showing the development of part of this model. Complete model development, along with validation with experimental data is reserved for future.

During experimentation, it has been observed that chips produced were very small particles like dust. The cutting grain model development will enable to evaluate the equivalent chip thickness, and will help to understand the possible phenomenon for formation of very small chip thickness. Through this model, it was possible to determine the selection of one parameter among feed rate and cutting velocity for material removal evaluation.

Furthermore, the correlation of chip compression ratio and shear strain rate can provide the better information of plastic deformation in metal cutting with thin discs.

4.1 Cutting Grain Model

In this section, the evolution of chip thickness in relation to undeformed chip thickness is determined and analysed by studying the position and velocity of the abrasive grains in their defined trajectory. Assuming the uniform distribution of grains on abrasive cut off wheel, the trajectory of single cutting grain is shown in figure 20. The distance between two consecutive grains has been defined to be the depth of cut or undeformed chip thickness.

In the defined trajectory 012 in figure 20, the cutting grain enters at point 1, and leaves at point 2. So, 1-2 is the distance covered by the grain along the thickness of the material e_m in relation to the downward displacement $V_f t$ by the cutting disc in y direction. Due to downward feed rate V_f, the distance between point 1 and 2 does not remain horizontal, and follows the curved path. R is the radial distance of the grain from the centre of the cutting disc. The cutting velocity V_c is defined in terms of radial distance R and rotational velocity of the cutting disc.

(α) is the angular position, that defines the path of cutting grain between points 1-2. Therefore, (α) include the interval (-α_o, α_o) that correspond to the angular position of point 1 and point 2 respectively.

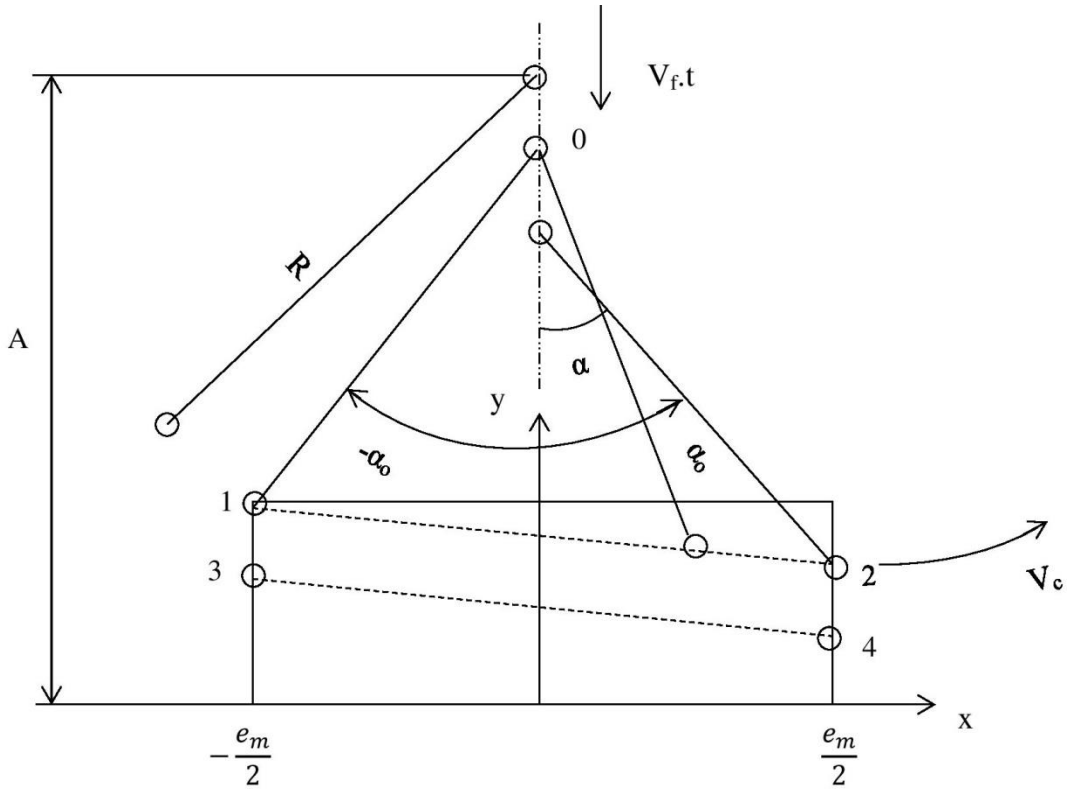

Figure 20. Cutting grain path

In the defined trajectory shown in figure 20, the position of cutting grain is resolved in to x and y components as

$$X = Rsin(\alpha) \tag{25}$$

$$Y = A - V_f.t - Rcos(\alpha) \tag{26}$$

From figure 20, it can be deduced that

$$X_2 - X_1 = e_m \tag{27}$$

Putting values of X_1, X_2 and replacing (α) with (-α_o) in X_1 and (α_o) in X_2, Eq. (25) becomes

$$sin\ (\alpha_o) = \frac{e_m}{2R} \tag{28}$$

For a very small value of (α_o), $\sin(\alpha_o) \approx (\alpha_o)$

$$(\alpha_o) = \frac{e_m}{2R} \tag{29}$$

In figure 20, $\Delta Y = Y_2 - Y_1$

Replacing values of ($-\alpha_o$) in Y_1 and (α_o) for Y_2 in Eq. (26), we have

$$\Delta Y = V_f\,(t_2 - t_1) \tag{30}$$

Taking derivative of Eq. (25) and Eq. (26) with respect to time

$$\dot{X} = R\,\dot{\alpha}\,cos(\alpha) \tag{31}$$

$$\dot{Y} = -V_f + R\,\dot{\alpha}\,sin\,(\alpha) \tag{32}$$

The magnitude of velocity vector V is

$$|V| = \sqrt{\dot{X}^2 + \dot{Y}^2} = \sqrt{R^2\dot{\alpha}^2 + {V_f}^2 - 2R\dot{\alpha}\,\mathrm{Sin}(\alpha)V_f} \tag{33}$$

$$|V| = \mathrm{R}\,\dot{\alpha}\sqrt{1 + (\frac{V_f}{\mathrm{R}\,\dot{\alpha}})^2 - \frac{2\,\mathrm{Sin}(\alpha)V_f}{R\dot{\alpha}}} \tag{34}$$

Where $R\,\dot{\alpha}$ is the cutting velocity V_c. The magnitude of cutting velocity V_c is much higher than the magnitude of V_f. So $\left(\frac{V_f}{V_c}\right)^2$ reduces nearly to zero, Eq. (34) becomes

$$|V| = V_c\sqrt{1 - \frac{V_f}{V_c}Sin(\alpha)} \tag{35}$$

Approximating with Taylor series, Eq. (35) reduces to

$$|V| = \mathrm{V_c}\left[1 - \frac{V_f}{\mathrm{V_c}}(\alpha)\right] \tag{36}$$

Length L is the distance covered by the grain from point 1 to 2; it can be expressed in terms of velocity and time as

$$L = \int V dt = \int V\frac{dt}{d\alpha}\,\mathrm{d}\alpha \tag{37}$$

Assuming the linear relationship between time t and angular velocity α, as the rotation velocity of the disc is constant

$t = m\alpha + b$, where m and b are constants, putting values for t_1 and t_2

$$m = \frac{t_2 - t_1}{2\alpha_o} \tag{38}$$

Putting the values of velocity V and m in Eq. (37), it becomes

$$L = \int_{-\alpha_o}^{\alpha_o} V_c \left[1 - \frac{V_f}{V_c}(\alpha)\right] \frac{t_2 - t_1}{2\alpha_o} d\alpha \tag{39}$$

Integrating Eq. (39),

$$L = V_c(t_2 - t_1) \tag{40}$$

Now putting the value of $(t_2 - t_1)$ from Eq. (40) to Eq. (30)

$$\Delta Y = L \frac{V_f}{V_c} \tag{41}$$

For this experiment, V_f is much lower than V_c, so ΔY approaches zero, which implies that L is approximately equal to e_m. As thickness of the material is very less, so it can be supposed that distance L follows the approximate linear path.

$$t_2 - t_1 \approx \frac{e_m}{V_c} \tag{42}$$

If the disc has only one cutting grain, then during one complete rotation of the cutting disc, the grain will again start cutting from (3) and will leave the material at point (4). Then y_1-y_3, which is the distance between two cutting grains, is the undeformed chip thickness, and is denoted as e_1. In the Eq.26, $y_1$and y_3 are obtained by replacing the value of α as 0 and 360^o simultaneously.

$$e_1 = V_f\ (t_o - t_3) \tag{43}$$

The time for one complete revolution of the cutting disc, if the rotation speed is constant

$$(t_o - t_3) = \frac{2\pi R}{V_c} \tag{44}$$

Where cutting velocity V_c is equal to 2πRn, n is the rotation speed of the cutting disc, so Eq. (43) becomes

$$e_1 = \frac{V_f}{n} \tag{45}$$

So the cutting depth is the function of feed rate and rotational speed of the cutting disc. The difference between y_2 and y_4 is supposed to be e_c, which is the equivalent cutting thickness.

4.1.1 Material removal rate

In this process through cutting grain, material removal can be function of cutting velocity V_c or feed rate V_f. In figure 21a, material removal rate is defined as the product of cutting velocity V_c and its perpendicular cross section $e_d\, e_c$. Where e_D is the thickness of cutting disc, and e_c is the equivalent cutting thickness. If it is the single cutting grain, thickness e_c equals e_1 defined in Eq.45. It is likely that there are more cutting grains, for this reason it is said as equivalent cutting thickness. In figure 21b, material removal rate is defined as the product of feed velocity V_f and its perpendicular cross section $e_D\, e_m$, where e_m is the thickness of the work piece.

Both material removal rates characterize the same volume of material removed per unit time, so

$$e_c = \frac{V_f e_m}{V_c} \tag{46}$$

Dividing 46 by 45, we can find the relationship between e_c and e_1

$$\frac{e_c}{e_1} = \frac{e_m}{\pi D} \tag{47}$$

The quotient is always less than 1. The diameter of the cutting disc is much greater than the thickness of the material. This is the evidence that the chip formation through cutting with thin abrasive discs is not characterized by single cutting grain. There are multiples grains on the periphery of the disc. All of the grains do not participate in the cutting process, some may rub and plough only, so probability of single cutting grain in material removal is very less, which makes the chip compression ratio very low. Assuming that the grains are equally spaced, the equivalent cutting thickness defined in Eq. 46 would be the characteristic thickness of the chip while cutting with thin abrasive discs. This equation indicates that increasing the cutting speed while keeping the feed rate constant will decrease the chip thickness. So the rate of material removed is

$$Q_c = V_f\, e_D\, e_m \tag{48}$$

It has been deduced during the chip thickness evaluation that in the case of low material thickness in comparison to cutting disc diameter, the trajectory of the cutting grain follows the linear path. The distance between the depths of two passing grains is the undeformed chip thickness. Equivalent cutting thickness could be result of many active cutting grains on the periphery of the disc. This is the first step to generate an upper bound shear model.

4.2 Upper bound theorem applied to orthogonal cutting

Upper bound theorem is used to estimate the forces to deform the body, by equating the rate of internal energy dissipation to the external forces. This estimate should be equal or higher than the correct force[101]. This method of analysis is to

1. Assumption of an internal flow field
2. Calculation of the rate at which this energy is consumed by this flow field
3. Calculation of external force by equating the rate of external work with the rate of internal energy consumption.

In this section, the shear strain rate in the primary deformation zone has been analyzed using the upper boundary theorem. Following assumptions have been considered while constructing velocity diagram or hodograph

1. The material is homogenous
2. Strain hardening is negligible
3. Interfaces are frictionless

4.2.1 Velocity Triangles

The deformation and friction energy spent in the cutting process are defined by velocity triangles[102]. The velocity triangles of orthogonal cutting by abrasive grit are shown in figure 22. A local rectangular coordinate system is set to show the direction of input and output velocities. An abrasive grain with depth of cut e_1, moving with cutting velocity V_c in y-z direction, produces plastic deformation in the shear plane y-y. The position of the shear plane is defined by the angel of shear or cutting angle Φ of abrasive grit. The movement of the grain is show by parallelogram ABCD, moving with velocity V_c. After crossing the shear plane, the parallelogram ABCD is distorted in to new parallelogram CDEF, moving with velocity of chip V_{ch} , following the rake face shape defined by rake angle α_o. The velocity diagram is shown in figure 22b. u is the component of velocity in x direction and V is the component of velocity in y direction. According to parallelogram law of velocities, it can be seen that chip velocity V_{ch} is the vector sum of shearing velocity V_s and cutting velocity V_c .

To understand the velocities in the shear plane, a corresponding hodograph is shown in figure 22a.This investigation is one dimensional approach and steady flow solution.

4.2.2 Shear zone model

Due to complexity of cutting process, it is very difficult to present the real model of the primary shear zone[102]. The models developed over the years differ in division of shear zone. Oxley proposed the idea that the shear zone occurs in a band of parallel faces, equidistant from the edges[103]. Astakhov [104]showed that the shear zone can be divided in to two unequal

parts, the first region is called wide region, where plastic deformation takes place at a low rate and the second region is narrow region where plastic deformation is at higher rate. Tounsi et al[105] reinforced the Astakhov's idea with the division of main shear plane in to two unequal parts characterized by portion r as shown in figure 22a, and deduced that the width of the cutting band h is equal to half of e_c.

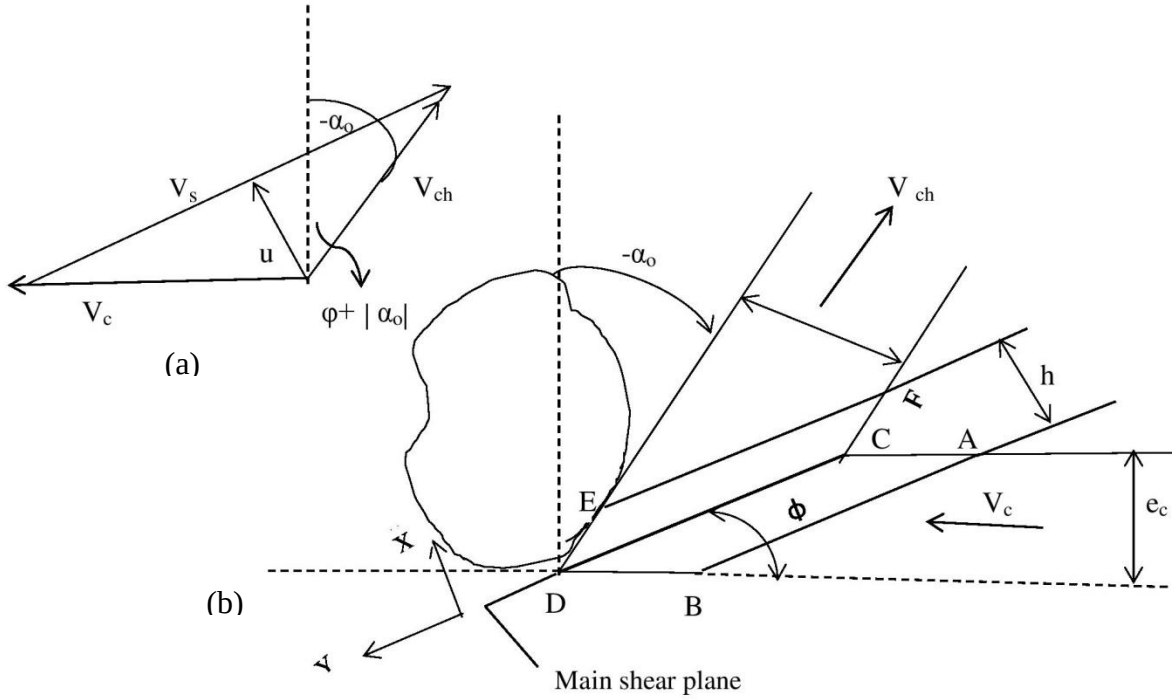

Figure 21. Orthogonal cutting of grain (a) Velocity triangles (b) Orthogonal cutting model

A model is presented in figure 21, shows that the plastic deformation occurs in a shear band of parallel faces. The figure 22a shows the speed at the entrance and exit of the parallel-sided face. The reference system is placed on the cutting plane. In figure 22b, a piecewise linear function for the shear strain rate is shown. Said behavior appearing within the cutting band has a maximum $\dot{Y}_s$ above the shear plane [105].

Where u and v are the components of the velocities in the x and y direction respectively. Components of the velocities at the entry and exit of the shear band are

$$u_o = |V_c| \sin \varphi \tag{49}$$

$$v_o = |V_c| \cos \varphi \tag{50}$$

$$u_1 = |V_{ch}| \cos(\Phi + |\alpha_o|) \tag{51}$$

$$V_1 = -|V_{ch}| \sin(\Phi + |\alpha_o|) \quad (52)$$

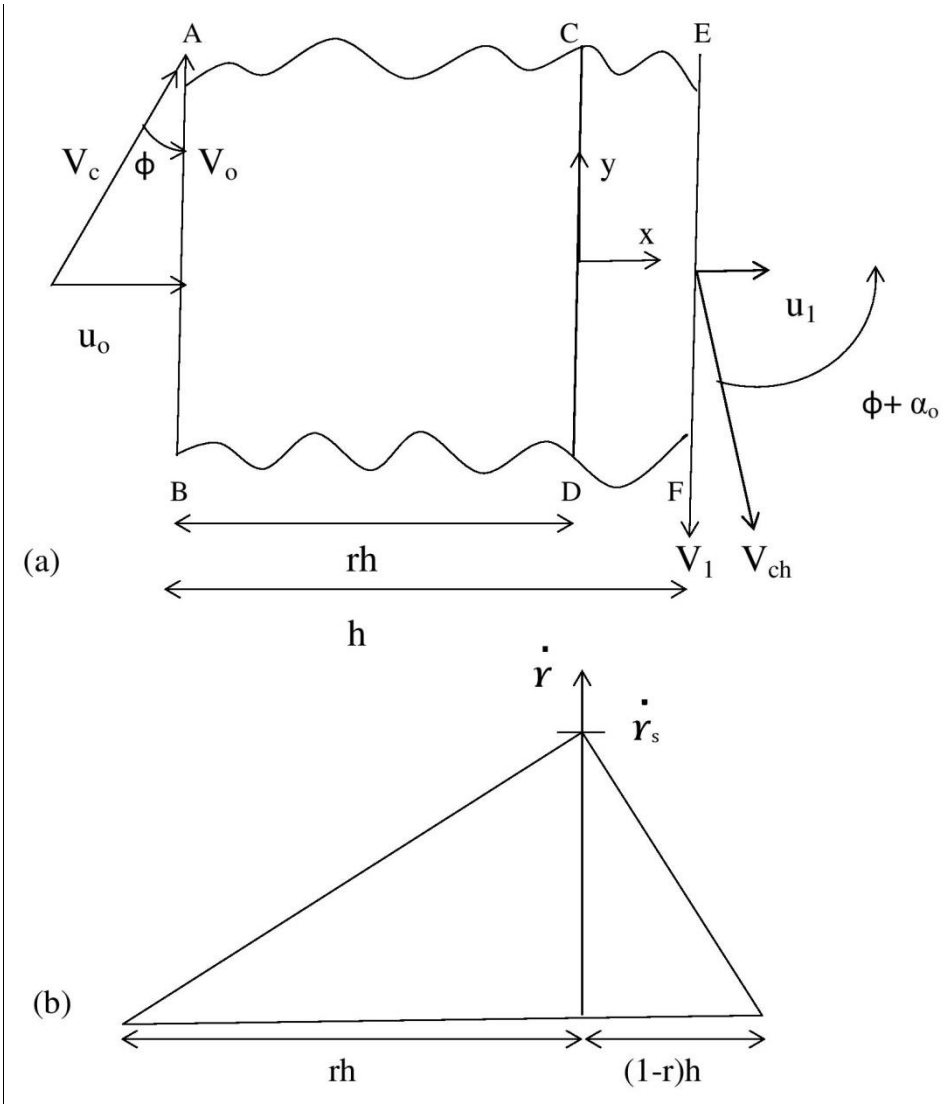

Figure 22 Shear zone model (a) Shear band of parallel faces (b) Shear strain rate distribution

Applying the one dimensional approach and steady flow solution, the velocity in the primary shear zone in x direction is only considered. The velocity field must satisfy the assumption of plastic incompressibility according to equation[102].

$$\frac{\partial u}{\partial x} + \frac{\partial v}{\partial y} = 0 \quad (53)$$

Since the velocity field in this case is represented as the function of x only, and equation of incompressibility proposes that normal component of velocity remains constant throughout the primary shear zone. So, Eq.53 reduces to

$$\frac{\partial u}{\partial x} = 0 \tag{54}$$

Therefore, in this coordinate system, the normal velocity component in the entry and exit band must be equal. Applying the equation of continuity, we have

$$u_o = u_1$$

$$|V_c| \sin \Phi = |V_{ch}| \cos(\Phi + |\alpha_o|) \tag{55}$$

$$\xi = \frac{|V_c|}{|V_{ch}|} = \frac{\cos(\Phi + |\alpha_o|)}{|V_c| \sin \Phi} \tag{56}$$

Where ξ is chip compression ratio

4.2.3 Equations of strain, and strain rate

The shear strain rate, and the maximum shear strain rate and velocity are analyzed in the primary shear zone. As plastic deformation in the ductile materials takes place by shearing process, this is the reason it is called primary shear zone[104]. So the chip formation in this model is considered mainly by shearing and material deformation does not takes places until it reaches the primary shear zone[102]. The transition from elastic to plastic deformation takes place in primary shear zone which is modeled as the shear band of constant thickness h. In the model, the thickness of the undeformed chip is thin compared to the width of the cut, so it is assumed that the chip is formed under plain strain condition. For a one-dimensional shear model, the strain tensor rate for the plain strain is given below. It has a unique non-zero term

$$\dot{\Upsilon} = \frac{\partial \mathrm{v}}{\partial \mathrm{x}} \tag{57}$$

Assuming that shear strain rate is maximum at the center of primary shear zone when x=0, then shear strain rate as function of maximum strain rate has the following form according to figure 22b.

$$\dot{\Upsilon}(x) = \dot{\Upsilon}_s \left(1 - \frac{x}{rh}\right) \quad -rh \le x \le 0 \tag{58a}$$

$$\dot{\Upsilon}(\dot{x}) = \dot{\Upsilon}_s \left(1 - \frac{x}{(1-r)h}\right) \quad 0 \le x \le (1-r)h \tag{58b}$$

These equations state the shear strain rate vanishes at the lower and upper bound of primary shear plane.

The relationship between velocity and strain rate is obtained by replacing Eq. (58) in Eq. (57), integrating with respect to x and applying the boundary conditions of velocity field.

$$v(x) = \dot{\Upsilon}_s \left(x + \frac{x^2}{2rh} + \frac{rh}{2}\right) + v_o \quad -rh \le x \le 0 \tag{59a}$$

$$v(x) = \dot{\Upsilon}_s \left(x - \frac{x^2}{2(1-r)h} - \frac{(1-r)h}{2}\right) + v_1 \quad 0 \le x \le (1-r)h \tag{59b}$$

At main shear plane, the tangential component of the velocity is zero[105]. So when *x=o*, the cutting velocity at the lower boundary of the shear plane is equal to the chip velocity of upper boundary of the shear plane. This implies that Eq.59b should be equal to Eq.59a.

$$\dot{\Upsilon}_s \frac{rh}{2} + v_o = -\dot{\Upsilon}_s \frac{(1-r)h}{2} + v_1 \tag{60}$$

$$\dot{\Upsilon}_s = \frac{2}{h}(v_1 - v_0) \tag{61}$$

Replacing Eq. (50), (52) and (56) in Eq. (61)

$$\dot{\Upsilon}_s = \frac{2}{h}|v_c\, cos(\Phi)[1 + tan\,\Phi)\, tan(\Phi + |\alpha_o|)] \tag{62}$$

On the other hand, *v(x=0) =0*, which allows us to obtain r from Eq. (59a)

$$r = \frac{v_o}{v_o - v_1} \tag{63}$$

Putting the values of v_o and v_1 in Eq. (61)

$$\mathrm{r} = \frac{1}{1+\tan\Phi\tan(\Phi+|\alpha_o|)} \tag{64}$$

On the other hand, shear strain rate is defined as time derivate of deformation

$$\dot{\Upsilon} = \frac{\mathrm{d}\Upsilon}{\mathrm{dt}} = \frac{\partial\Upsilon}{\partial \mathrm{x}} \frac{\partial \mathrm{x}}{\partial \mathrm{t}} = u\frac{\partial\Upsilon}{\partial \mathrm{x}} \tag{65}$$

Replacing Eq. (59) in Eq. (61), and differentiating with condition $\Upsilon(x = -rh) = \Upsilon(x = (1-\Upsilon)h)=0$

$$\dot{\Upsilon} = \frac{\dot{\Upsilon}_s}{u}\left(x - \frac{x^2}{2rh} + \frac{3rh}{2}\right) \qquad -rh \le x \le 0 \tag{66}$$

$$\frac{\dot{\gamma}_s}{u}\left(x-\frac{x^2}{2(1-r)h}-\frac{(1-r)h}{2}\right) \qquad 0 \le x \le (1-r)h \tag{67}$$

As depicted in Eq. (62) and Eq. (66) that maximum shear strain rate and shear strain rate are the functions of cutting velocity, rake angle and angle of shear cutting plane. The proposed model divides the shear plane in to two zones, the shear strain rate is zero at the entry boundary, and reaches the maximum value at the main shear plane. After crossing the main shear plane, the shear strain rate again reduces and vanishes at exit boundary. The division of shear zone depends on the fraction r, which is the function of rake angle and angle of cutting plane.

4.3 Conclusion

The model of single cutting grain is proposed to study the grain interaction with work piece to produce the chip. Defining the distance between two consecutive grains as the depth of cut, the chip thickness is analyzed by studying the grain trajectory. Due to low material thickness, the grain trajectory followed the linear path. The chip thickness in relation to depth of cut was found to be very low, which suggested that chip formation could be a result of many cutting grains located on the periphery of the cutting disc. So, feed rate and its perpendicular section i.e, thickness of the cutting disc and material thickness turned out to be more suitable parameters to evaluate the material removal rate.

Defining the distance between two grains as the depth of cut, the upper bound model is applied to the orthogonal cutting of grains to study the shear strain at the primary deformation zone. The model proposed that material deformation takes places in the parallel sided zone of constant thickness. The shear strain rate distribution is linear, and maximum shear strain rate is at the center of the shear plane. The division of shear band around the main shear plane is a function of rake angle and angle of cutting plane. Up until now, this is the theoretical development of model. To accurately predict the behavior of this model in comparison to previous studies and the evaluation of shear strain rate and maximum shear rate by validating the model with the experimental data is the future work.

Chapter 5 Conclusions and Future Work Recommendations

5.1 Conclusion

Through the research carried out on abrasive metal cutting with thin discs, following general conclusions can be drawn.

1. The state of art designed and manufactured equipment allowed the precise and smooth cutting of specimen at a predefined feed rate. The feed rate controls, movement and position of stepper motor has been programmed and executed through microcontroller Arduino.

2. Characterization of commercially available standard grinders and cutting discs in terms of energy consumption has been achieved by adopting an innovative methodology. The calibration of standard angle grinder on test bench allowed evaluating the relationship between cutting power, and electrical energy consumption. Devising an alternative way to measure the cutting power eliminated the need to separately measure the cutting force, and cutting velocity during the process. The cutting power equation can be repeatedly used for the same grinder; hence adopted methodology to measure SEC provides more easiness and is efficient.

3. The SEC, an indicator of energy efficiency and machinability of materials has been measured, categorized in to components of sliding, plowing and cutting through empirical model. The specific energy consumption is a function of material properties, process parameters and cutting tool configuration.

4. The comprehensive model of specific energy consumption on the basis of primary and secondary rubbing energies, specific plowing energy and specific cutting energy is developed for cubitron grits of triangular pyramidal shape. The specific energy modeling in to components revealed that specific plowing energy is more sensitive to material removal rate in comparison to sliding energy. Specific plowing energy is varying inversely with the square of material removal rate, means a small change in material removal rate is an indicative of huge change in specific plowing energy. The model also helped to find out the contribution of specific energy components with change in material removal rate. The model validation on experimental data for materials reveled that mechanical properties of the materials also play a significant role in appearance, absence or dominance of specific energy components.

5. The single cutting grain model is presented based on the trajectory of the cutting grain. The cutting grain follows the linear path due to low material thickness. Equivalent cutting thickness was found to be very low in comparison to the depth of cut, so it was concluded that it is not

possible to characterize the chip thickness using the single cutting grain model. The chip formation could be the result of many cutting grains present on the periphery of the cutting wheel. It was deduced that feed rate is more suitable parameter to evaluate the material removal rate. Applying the upper bound theorem, a model was proposed to determine the shear strain based on division of shear plane by a band with parallel faces. The distribution of shear strain was initially proposed to be linear and was found to be the function of shear plane angle, rake angle and cutting velocity.

6. Machinability of materials is largely affected by the grain shape and type, mechanical properties and cutting conditions. With this experimental set up, using the standard disc for materials, the machining of brittle materials was found to be easier. Using semi super abrasive cubitron disc, redundant energies of sliding and plowing were reduced, which is an indication of better machinability of materials.

5.2 Future work recommendations

1. The shear distribution model developed in this study will be validated with cutting conditions of different materials. The correlation of chip compression ratio, with shear strain can provide the better understanding about plastic deformation. Moreover, the temperature distribution in the primary shear plane can also be obtained by developing the heat transfer equation. Calculating the shear stress on the main shear plane, cutting forces in the primary deformation zone can also be evaluated.

2. As abrasive cut off operation is performed at very high cutting velocities and feed rates, and correct visualization of specific energy components was only possible through mathematical model. The future work could be the FEM analysis of the process to simulate the formation of scratch in sliding phase, followed by grain indentation in plowing and SCE phases. This will help to visualize the transition in three stages as well as impact of grain geometry on SEC components.

3. In this research, feed rate has been considered as the only process parameter, and cutting was performed at the constant cutting velocity. In future, variable speed grinder can be used to analyze the influence of cutting velocity and feed rate on SEC. In addition, neural network technique can be used for optimization of process parameters to minimize the energy use.

4. Although abrasive disc are continuously consumed during the abrasive cut off process, but cutting conditions and material properties influence the tool wear. Future work could be the development of model to predict tool wear relationship with cutting conditions.

5. Using deep learning algorithms, energy consumption behavior at higher feed rates can be predicted. This could be achieved by first processing the given experimental data using ANN to detect anomaly, and then purified data will be forecasted for higher feed rates. Constraints could be tool life, and temperature increment at the grinding zone.

References

1. Abebe M, Appl FC (1988) Theoretical analysis of the basic mechanics of abrasive processes. Part I: General model. Wear 126:251–266 . https://doi.org/10.1016/0043-1648(88)90169-X

2. Metal Cutting Theory and Practice - 3rd Edition - David A. Stephenson. https://www.routledge.com/Metal-Cutting-Theory-and-Practice/Stephenson-Agapiou/p/book/9780367868192. Accessed 2 Mar 2021

3. Malkin S (2013) Grinding Processes. In: Encyclopedia of Tribology. Springer US, pp 1573–1580

4. Neugebauer R, Hess KU, Gleich S, Pop S (2005) Reducing tool wear in abrasive cutting. Int J Mach Tools Manuf 45:1120–1123 . https://doi.org/10.1016/j.ijmachtools.2005.01.002

5. Shaw MC, Cookson JO (2005) Metal cutting principles (Vol. 2). Dairy Sci Technol CRC Taylor Fr Gr 759

6. Shaw MC (Milton C (1996) Principles of abrasive processing. Clarendon Press

7. Nelson JA, Westrich RM (1974) Abrasive Cutting in Metallography. In: Metallographic Specimen Preparation. pp 41–54

8. Hou ZB, Komanduri R (2003) On the mechanics of the grinding process - Part I. Stochastic nature of the grinding process. Int J Mach Tools Manuf 43:1579–1593 . https://doi.org/10.1016/S0890-6955(03)00186-X

9. Shaw MC, Farmer DA, Nakayama K (1967) Mechanics of the abrasive cutoff operation. J Manuf Sci Eng Trans ASME 495–502 . https://doi.org/10.1115/1.3610096

10. Shaw MC (1975) The rating of abrasive cutoff wheels. J Manuf Sci Eng Trans ASME 97:138–146 . https://doi.org/10.1115/1.3438526

11. Eshghy S (1967) Thermal aspects of the abrasive cutoff operation. Part 1-theoretical analysis. J Manuf Sci Eng Trans ASME 89:356–360 . https://doi.org/10.1115/1.3610052

12. Hou ZB, Komanduri R (2004) On the mechanics of the grinding process, Part III - Thermal analysis of the abrasive cut-off operation. Int J Mach Tools Manuf 44:271–289 . https://doi.org/10.1016/j.ijmachtools.2003.09.009

13. Kannappan S, Malkin S (1972) Effects of grain size and operating parameters on the mechanics of grinding. J Manuf Sci Eng Trans ASME 833–842 . https://doi.org/10.1115/1.3428258

14. Zhong ZW, Venkatesh VC (2009) Recent developments in grinding of advanced

materials. Int J Adv Manuf Technol 41:468–480 . https://doi.org/10.1007/s00170-008-1496-3

15. Kannappan S, Malkin S (1972) Effects of grain size and operating parameters on the mechanics of grinding. J Manuf Sci Eng Trans ASME 94:833–842 . https://doi.org/10.1115/1.3428258

16. Rowe WB (2013) Principles of modern grinding technology

17. Shaw MC (1980) PRINCIPLES OF MATERIAL REMOVAL. Proc - Comput Netw Symp 1:227–253 . https://doi.org/10.1016/B978-1-4832-8414-9.50018-3

18. Malkin S (1984) Grinding of metals: Theory and application. J Appl Metalwork 1984 32 3:95–109 . https://doi.org/10.1007/BF02833688

19. Ghosh S, Chattopadhyay AB, Paul S (2008) Modelling of specific energy requirement during high-efficiency deep grinding. Int J Mach Tools Manuf 48:1242–1253 . https://doi.org/10.1016/j.ijmachtools.2008.03.008

20. Rasim M, Mattfeld P, Klocke F (2015) Analysis of the grain shape influence on the chip formation in grinding. J Mater Process Technol 226:60–68 . https://doi.org/10.1016/j.jmatprotec.2015.06.041

21. Butler-Smith P, Axinte D, Daine M, Kong MC (2014) Mechanisms of surface response to overlapped abrasive grits of controlled shapes and positions: An analysis of ductile and brittle materials. CIRP Ann / Int Inst Prod Eng Res 63:321–324

22. Öpöz TT, Chen X (2012) Experimental investigation of material removal mechanism in single grit grinding. Int J Mach Tools Manuf 63:32–40 . https://doi.org/10.1016/j.ijmachtools.2012.07.010

23. Setti D, Ghosh S, Rao PV (2017) A method for prediction of active grits count in surface grinding. Wear 382–383:71–77 . https://doi.org/10.1016/j.wear.2017.04.012

24. Jamshidi H, Gurtan M, Budak E (2019) Identification of active number of grits and its effects on mechanics and dynamics of abrasive processes. J Mater Process Technol 273:116239 . https://doi.org/10.1016/j.jmatprotec.2019.05.020

25. Pang J, Wu C, Wang Q, Li B (2018) Modeling of grinding wheel topography based on a joint method of 3D microscopic observation and embedded grindable thermocouple technique. Int J Adv Manuf Technol 97:25–37 . https://doi.org/10.1007/s00170-018-1892-2

26. IEO (2018) International Energy Outlook 2018 (IEO2018) Key takeaways. In: U.S. Energy Inf. Adm.

27. Rahimifard S, Seow Y, Childs T (2010) Minimising embodied product energy to support energy efficient manufacturing. CIRP Ann - Manuf Technol 59(1):25–28 . https://doi.org/10.1016/j.cirp.2010.03.048

28. Yuan C, Zhai Q, Dornfeld D (2012) A three dimensional system approach for environmentally sustainable manufacturing. CIRP Ann - Manuf Technol 61:39–42 . https://doi.org/10.1016/j.cirp.2012.03.105

29. Yingjie Z (2014) Energy efficiency techniques in machining process: A review. Int. J. Adv. Manuf. Technol. 71(5–8):1123-1132.

30. He Y, Liu F, Wu T, Zhong FP, Peng B (2012) Analysis and estimation of energy consumption for numerical control machining. Proc Inst Mech Eng Part B J Eng Manuf 226:255-266. . https://doi.org/10.1177/0954405411417673

31. Malkin, S. and CG (2008) Grinding technology: theory and applications of machining with abrasives. New York: Industrial Press.

32. Ding H, Guo D, Cheng K, Cui Q (2014) An investigation on quantitative analysis of energy consumption and carbon footprint in the grinding process. Proc Inst Mech Eng Part B J Eng Manuf 228:950–956 . https://doi.org/10.1177/0954405413508280

33. Komanduri R, Iyengar S (2001) Conventional and Super Abrasive Materials. In: Encyclopedia of Materials: Science and Technology. pp 1629–1651

34. R.S. Hahn, On the nature of the grinding process,... - Google Scholar. https://scholar.google.com/scholar?hl=en&as_sdt=0%2C5&q=R.S.+Hahn%2C+On+the+nature+of+the+grinding+process%2C+in%3A+Proceedings+of+the+3rd+International+Machine+Tool+Design+%26+Research+Conference%2C+Manchester%2C+1962%2C+pp.+129–154&btnG=. Accessed 26 Mar 2021

35. Öpöz TT, Chen X (2012) Experimental investigation of material removal mechanism in single grit grinding. Int J Mach Tools Manuf 63:32–40 . https://doi.org/10.1016/j.ijmachtools.2012.07.010

36. Stephen Malkin CG (1989) Grinding Technology: Theory and Application of Machining with Abrasives. Ellis Horwood Limited

37. Sinha MK, Ghosh S, Paruchuri VR (2019) Modelling of specific grinding energy for Inconel 718 superalloy. Proc Inst Mech Eng Part B J Eng Manuf 233:443–460 . https://doi.org/10.1177/0954405417741513

38. Singh V, Venkateswara Rao P, Ghosh S (2012) Development of specific grinding energy model. Int J Mach Tools Manuf 60:1–13 . https://doi.org/10.1016/j.ijmachtools.2011.11.003

39. (4) (PDF) An Improved Model for Specific Energy Estimation in Surface Grinding of Inconel 718. https://www.researchgate.net/publication/286932438_An_Improved_Model_for_Specific_Energy_Estimation_in_Surface_Grinding_of_Inconel_718. Accessed 11 Apr 2021

40. Dai C, Ding W, Xu J, Fu Y, Yu T (2017) Influence of grain wear on material removal behavior during grinding nickel-based superalloy with a single diamond grain. Int J Mach

Tools Manuf 113:49–58 . https://doi.org/10.1016/j.ijmachtools.2016.12.001

41. Rubenstein C (1972) The mechanics of grinding. Int J Mach Tool Des Res 12:127–139 . https://doi.org/10.1016/0020-7357(72)90028-5

42. Singh V, Patnaik Durgumahanti US, Venkateswara Rao P, Ghosh S (2011) Specific ploughing energy model using single grit scratch test. Int J Abras Technol 4:156–173 . https://doi.org/10.1504/IJAT.2011.041609

43. Sinha MK, Ghosh S, Paruchuri VR (2019) Modelling of specific grinding energy for Inconel 718 superalloy. Proc Inst Mech Eng Part B J Eng Manuf 233:443–460 . https://doi.org/10.1177/0954405417741513

44. Patnaik Durgumahanti US, Singh V, Venkateswara Rao P (2010) A New Model for Grinding Force Prediction and Analysis. Int J Mach Tools Manuf 50:231–240 . https://doi.org/10.1016/j.ijmachtools.2009.12.004

45. Matsuo T, Toyoura S, Oshima E, Ohbuchi Y (1989) Effect of Grain Shape on Cutting Force in Superabrasive Single-Grit Tests. CIRP Ann - Manuf Technol 38:323–326 . https://doi.org/10.1016/S0007-8506(07)62714-0

46. Singh V, Ghosh S, Rao PV (2011) Comparative study of specific plowing energy for mild steel and composite ceramics using single grit scratch tests. Mater Manuf Process 26:272–281 . https://doi.org/10.1080/10426914.2010.526979

47. Stachowiak GW, Batchelor, Andrew W GB (2004) Experimental methods in tribology: Introduction. Tribol. Ser.

48. Malkin S, Joseph N (1975) Minimum energy in abrasive processes. Wear 32:15–23 . https://doi.org/10.1016/0043-1648(75)90201-X

49. Rowe WB (2018) Towards high productivity in precision grinding. Inventions 3(2):24

50. Nápoles Alberro A, González Rojas H, Sánchez Egea A, Hameed S, Peña Aguilar R (2019) Model Based on an Effective Material-Removal Rate to Evaluate Specific Energy Consumption in Grinding. Materials (Basel) 12:939 . https://doi.org/10.3390/ma12060939

51. Masoumi H, Safavi SM, Salehi M (2014) Grinding force, specific energy and material removal mechanism in grinding of HVOF-sprayed WC-Co-Cr coating. Mater Manuf Process 29:321–330 . https://doi.org/10.1080/10426914.2013.872261

52. Shaw MC (1996) Energy Conversion in Cutting and Grinding*. CIRP Ann - Manuf Technol 45:101–104 . https://doi.org/10.1016/S0007-8506(07)63025-X

53. Turchetta S (2010) Cutting force in stone machining by diamond disk. Adv Mater Sci Eng 2010: . https://doi.org/10.1155/2010/631437

54. Azizi A, Mohamadyari M (2015) Modeling and analysis of grinding forces based on the single grit scratch. Int J Adv Manuf Technol 78:1223–1231 .

https://doi.org/10.1007/s00170-014-6729-z

55. Brach K, Pai DM, Ratterman E, Shaw MC (1988) Grinding forces and energy. J Manuf Sci Eng Trans ASME 110:25–31 . https://doi.org/10.1115/1.3187838

56. Jain VK, Mote RG (2005) On the temperature and specific energy during electrodischarge diamond grinding (EDDG). Int J Adv Manuf Technol 26:56–67 . https://doi.org/10.1007/s00170-003-1983-5

57. Villagomez-Galindo M, Carbajal-De La Torre G, Romo-Castañeda JC, Bedolla-Jacuinde A, González-Rojas HA, Espinosa-Medina MA (2016) Casting Fe-Al-based intermetallics alloyed with Li and Ag. J Mater Res 31:2473–2481 . https://doi.org/10.1557/jmr.2016.249

58. 3M (2020) 3M, "Cut and grind wheel." https://www.3m.com/3M/en_US/metalworking-us/applications/cutting/, Website Accessed:2020-03-10. Accessed 3 Mar 2020

59. Wurm JD (1984) Machinist (AFSC 42750). Extension Course Institute, Air University

60. Sivasankar B (2008) Engineering chemistry. Tata McGrawHill New Delhi

61. García de Jalón J (1994) Kinematic and Dynamic Simulation of Multibody Systems The Real-Time Challenge

62. Gutowski T, Dahmus J, Thiriez A (2006) Electrical energy requirements for manufacturing processes. In: Proceedings of the 13th CIRP International Conference on Life Cycle Engineering, LCE 2006. pp 623–638

63. Kara S, Li W (2011) Unit process energy consumption models for material removal processes. CIRP Ann - Manuf Technol 37–40 . https://doi.org/10.1016/j.cirp.2011.03.018

64. Li W, Winter M, Kara S, Herrmann C (2012) Eco-efficiency of manufacturing processes: A grinding case. CIRP Ann - Manuf Technol 61:59–62 . https://doi.org/10.1016/j.cirp.2012.03.029

65. Marinescu ID, Rowe WB, Dimitrov B, Inasaki I (2004) Tribology of Abrasive Machining Processes

66. Verhoeven J (2007) Steel Metallurgy for the Non-Metallurgist. ASM International

67. Larson B (2003) Collaboration for Nondestructive Testing Education — Extending the Reach. pp 1899–1904

68. Astakhov VP, Outeiro JC (2008) Metal cutting mechanics, finite element modelling. In: Machining: Fundamentals and Recent Advances. pp 1–27

69. Buehler MJ (2008) Atomistic modeling of materials failure

70. Yousefi R, Ichida Y (2000) Study on ultra-high-speed cutting of aluminum alloy: Formation of welded metal on the secondary cutting edge of the tool and its effects on the quality of finished surface. Precis Eng 24:371–376 . https://doi.org/10.1016/S0141-

6359(00)00048-9

71. Hameed S, Rojas HAG, Benavides JIP, Alberro AN, Egea AJS (2018) Influence of the regime of electropulsing-assisted machining on the plastic deformation of the layer being cut. Materials (Basel). https://doi.org/10.3390/ma11060886

72. Morris DG, Muñoz-Morris MA, Requejo LM (2007) Work hardening in Fe-Al alloys. Mater Sci Eng A 460:163–173 . https://doi.org/10.1016/j.msea.2007.01.014

73. Liu CT, George EP, Maziasz PJ, Schneibel JH (1998) Recent advances in B2 iron aluminide alloys: Deformation, fracture and alloy design. Mater Sci Eng A 258:84–98 . https://doi.org/10.1016/S0921-5093(98)00921-6

74. Saigal A, Yang W (2003) Analysis of milling of iron aluminides. J Mater Process Technol 132:149–156 . https://doi.org/10.1016/S0924-0136(02)00843-9

75. Zhang T, Jiang F, Yan L, Xu X (2018) Research on the Size Effect of Specific Cutting Energy Based on Numerical Simulation of Single Grit Scratching. J Manuf Sci Eng Trans ASME 140: . https://doi.org/10.1115/1.4039916

76. Linke B, Garretson I, Torner FM (2017) UC Davis UC Davis Previously Published Works Title Grinding energy modeling based on friction, plowing and shearing Publication Date. https://doi.org/10.1115/1.4037239

77. Wu C, Li B, Yang J, Liang SY (2016) Prediction of grinding force for brittle materials considering co-existing of ductility and brittleness. Int J Adv Manuf Technol 87:1967–1975 . https://doi.org/10.1007/s00170-016-8594-4

78. Kupka M (2006) High temperature strengthening of the FeAl intermetallic phase-based alloy. Intermetallics 14:149–155 . https://doi.org/10.1016/j.intermet.2005.04.013

79. George EP, Baker I (1998) Thermal vacancies and the yield anomaly of FeAl. Intermetallics 6:759–763 . https://doi.org/10.1016/s0966-9795(98)00063-6

80. Awan MR, Rojas HAG, Benavides JIP, Hameed S (2021) Experimental technique to analyze the influence of cutting conditions on specific energy consumption during abrasive metal cutting with thin discs. Adv Manuf 2021 1–12 . https://doi.org/10.1007/S40436-021-00361-2

81. Fang L, Xing J, Liu W, Xue Q, Wu G, Zhang X (2001) Computer simulation of two-body abrasion processes. Wear 250:1356–1360 . https://doi.org/10.1016/S0043-1648(01)00769-4

82. Franco LA, Sinatora A (2017) Material removal factor (fab): A critical assessment of its role in theoretical and practical approaches to abrasive wear of ductile materials. Wear 382–383:51–61 . https://doi.org/10.1016/J.WEAR.2017.04.006

83. Batako ADL, Morgan MN, Rowe BW (2012) High efficiency deep grinding with very high removal rates. Int J Adv Manuf Technol 2012 669 66:1367–1377 .

https://doi.org/10.1007/S00170-012-4414-7

84. Marinescu ID, Rowe B, Ling Y, Wobker HG (2015) Abrasive Processes. In: Handbook of Ceramics Grinding and Polishing. Elsevier, pp 67–132

85. (2015) Handbook of Ceramics Grinding and Polishing. Handb Ceram Grind Polishing. https://doi.org/10.1016/C2011-0-04219-9

86. Kompella S, Zhang K IMPROVED SUPERALLOY GRINDING PERFORMANCE WITH NOVEL CBN CRYSTALS

87. Tso PL (1995) Study on the grinding of Inconel 718. J Mater Process Technol 55:421–426 . https://doi.org/10.1016/0924-0136(95)02026-8

88. Abachi P, Naseri PSZ, Coyle KP and TW (2016) Fracture Behavior Evaluation of High-Strength 7050 and 7075 Aluminum Alloys Using V-Notched Specimen. Fract Mech - Prop Patterns Behav. https://doi.org/10.5772/64463

89. Precision Abrasive Grinding in the 21st Century: Conventional, Ceramic, Semi ... - Harry G. Sachsel, C.A.E. - Google Books. https://books.google.es/books?id=3bgJQRkE7lgC&pg=PA496&lpg=PA496&dq=CBN+and+cubitron+are+the+same&source=bl&ots=r562sVtD0M&sig=ACfU3U0nqenWN8iTuHz6uMivITFzfME1FQ&hl=en&sa=X&ved=2ahUKEwiHiO6wg8zyAhUDxoUKHQj1BWsQ6AF6BAgxEAM#v=onepage&q=CBN and cubitron are the same&f=false. Accessed 25 Aug 2021

90. Aluminum 1100-O. http://www.matweb.com/search/datasheet_print.aspx?matguid=db0307742df14c8f817bd8d62207368e. Accessed 11 May 2021

91. Copper, Cu; Annealed. http://www.matweb.com/search/datasheet_print.aspx?matguid=9aebe83845c04c1db5126fada6f76f7e. Accessed 26 Aug 2021

92. Liu H, Zhang J, Xu X, Jiang Y, He Y, Zhao W (2016) Effect of microstructure evolution on chip formation and fracture during high-speed cutting of single phase metals. Int J Adv Manuf Technol 2016 911 91:823–833 . https://doi.org/10.1007/S00170-016-9823-6

93. Advanced Machining Processes: Innovative Modeling Techniques - Google Books. https://books.google.es/books?id=PhBADwAAQBAJ&pg=PT59&lpg=PT59&dq=fracture+of+Al+1100+during+machining&source=bl&ots=-Fkmwq46VQ&sig=ACfU3U1wqJcbQ_x5ETgktoRQdVaD1CdtNg&hl=en&sa=X&ved=2ahUKEwiPwPb4ss_yAhWGSsAKHQI6BFcQ6AF6BAgkEAM#v=snippet&q=dislocation&f=false. Accessed 26 Aug 2021

94. Huang S, Khan AS (1992) Modeling the mechanical behaviour of 1100-0 aluminum at different strain rates by the bodner-partom model. Int J Plast 8:501–517 . https://doi.org/10.1016/0749-6419(92)90028-B

95. Ni H, Elmadagli M, Alpas AT (2004) Mechanical properties and microstructures of 1100 aluminum subjected to dry machining. Mater Sci Eng A 385:267–278 . https://doi.org/10.1016/J.MSEA.2004.06.048

96. Öpöz TT, Chen X (2012) Experimental investigation of material removal mechanism in single grit grinding. Int J Mach Tools Manuf 63:32–40 . https://doi.org/10.1016/J.IJMACHTOOLS.2012.07.010

97. Patil D V., Ghosh S, Ghosh A, Chattopadhyay AK, Chattopadhyay AB (2007) On grindability of Inconel 718 under high efficiency deep grinding by monolayer cBN wheel. Int J Abras Technol 1:173–186 . https://doi.org/10.1504/IJAT.2007.015382

98. Shah GN, Bell AC, Malkin S (1977) Quantitative characterization of abrasive surfaces using a new profile measuring system. Wear 41:315–325 . https://doi.org/10.1016/0043-1648(77)90011-4

99. Law SS, Wu SM (1973) Simulation Study of the Grinding Process. J Eng Ind 95:972–978 . https://doi.org/10.1115/1.3438277

100. Ghosh S, Chattopadhyay AB, Paul S (2008) Modelling of specific energy requirement during high-efficiency deep grinding. Int J Mach Tools Manuf 48:1242–1253 . https://doi.org/10.1016/j.ijmachtools.2008.03.008

101. Bower AF (2009) Applied Mechanics of Solids. Appl Mech Solids 1–795 . https://doi.org/10.1201/9781439802489

102. Li B, Wang X, Hu Y, Li C (2010) Analytical prediction of cutting forces in orthogonal cutting using unequal division shear-zone model. Int J Adv Manuf Technol 2010 545 54:431–443 . https://doi.org/10.1007/S00170-010-2940-8

103. Palmer WB, Oxley PLB (2006) Mechanics of Orthogonal Machining: http://dx.doi.org/101243/PIME_PROC_1959_173_053_02 173:623–654 . https://doi.org/10.1243/PIME_PROC_1959_173_053_02

104. Astakhov VP, Osman MOM, Hayajneh MT (2001) Re-evaluation of the basic mechanics of orthogonal metal cutting: velocity diagram, virtual work equation and upper-bound theorem. Int J Mach Tools Manuf 41:393–418 . https://doi.org/10.1016/S0890-6955(00)00084-5

105. Tounsi N, Vincenti J, Otho A, Elbestawi MA (2002) From the basic mechanics of orthogonal metal cutting toward the identification of the constitutive equation. Int J Mach Tools Manuf 42:1373–1383 . https://doi.org/10.1016/S0890-6955(02)00046-9

Appendix I

I.1 Manufacturing of Machine

For this research, a kinematic structure has been designed to mount and move standard grinder on different down feed rates to cut different materials with cut off wheels. The parameters that are taken in to consideration for the design are the structure ability for dynamic loading, length of the links, speed and torque of the stepper motor. Stepper motor has been preferred for its ability to provide précised angular motion and hold position.

I.2 Description of Machine Components

1. Stepper Motor Drive

The speed and direction of stepper motor is controlled with drive, and is controlled with step modes. Step modes are a determining factor of the stepper motor's output torque and its resolution (the amount of degrees the motor shaft rotates per pulse). The drive used in this circuit has the option for micro stepping; it controls the current in the motor winding to a degree that further subdivides the number of positions between poles, subsequently dividing a full step into smaller steps.

2. Circuit details

Figure 23 shows the components used to make the machine circuit.

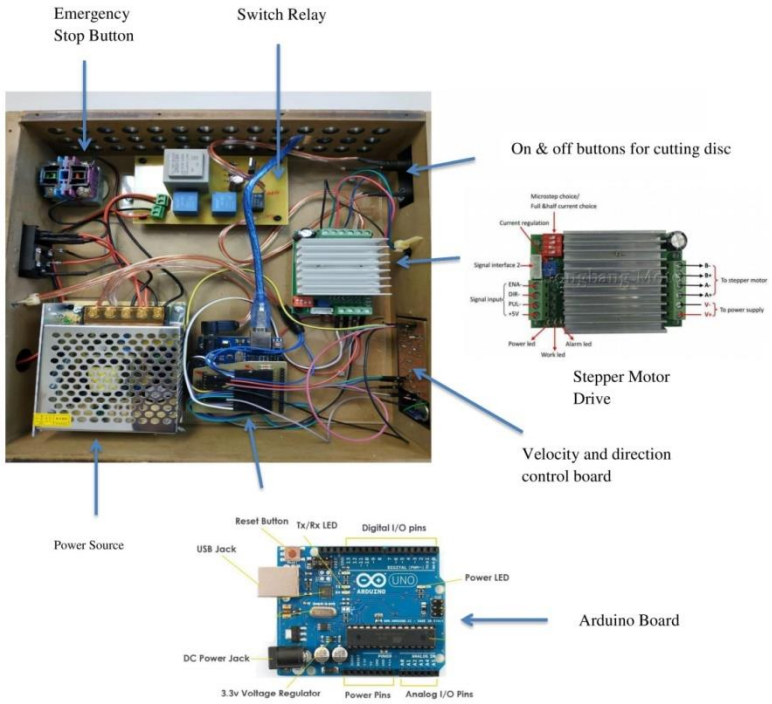

Figure 23 Machine components

The circuit consisting of LEDs, resistors and capacitors is programmed with PLC. PLC stores and processes input data from switches and potentiometer, and triggers the signals to the Arduino .Power source is used to step down the input voltage supply to 12V for stepper motor drive and other functions. It sends the output power consumed by the machine to power analyzer. Relays are used are used to control on and off switches of the circuit. When the current or voltage exceeds the threshold value, it activates the switch mechanism through the magnetic coil, which operates either to close the open contacts or open the close contacts.

3. Arduino

Arduino is the open source platform to build electronic projects, it contains physical programmable board (called as microcontroller) and software for code writing on computer and uploading it on the physical board. Arduino can be used to control motors, LEDs, Speakers, cameras etc. In this project stepper motor, LEDs and all motion controls buttons are programed with Arduino.

4. Arduino Program

```
int led1 = 5; //led 1 is connected to pin #4 (avoid pins 0 and 1 as they are used for serial communication)
int led2 = 6; //led2 is connected to pin #5
int led3 = 7; //etc
int led4 = 4;
int led5 = 11; //Led UP
int led6 = 8;  //led down
int Ab = 1;
int Dir = 3; //
int Step = 2; //
boolean state  = true;
int Vel =600;
const int SW1=10;  //Switch UP
const int SW2=9;   //Switch Down
bool state1 = LOW;
bool state2 = LOW;
const int LMUP=13;
const int LMDW=12;
int val=LOW;
int pot = A1; // potentiometer is connected to analog pin 1

int value;
```

As the first step, it is necessary to declare all the variables of LEDs, Switches, motor controls and Potentiometer. The initial state of switches is also defined.

For instance, int led4 = 4; Defines a variable whose name is LED, whose value is 4 and whose type is integer.

A Bool state holds one of two values true or false. Here Bool state 1 and 2 showing that initial state of the switches are false or low

```
void setup(){
pinMode(led1, OUTPUT); //assiging the led as an output
pinMode(led2, OUTPUT);
```

Void setup ()

This is a declaration for a function called "setup". . The “Setup” - where you layout the initial conditions for the program so that the Arduino knows what kind of work its going to be done. The code inside setup ()'s curly brackets ({and}) runs once at the very beginning of program and then never again.

Pin Mode Configures the specified pin to behave either as an input or an output.

Digital Write function writes a high or low value to a digital pin.

```
pinMode(led3, OUTPUT);
pinMode(led4, OUTPUT);
pinMode(led5, OUTPUT);
pinMode(led6, OUTPUT);
pinMode(pot, INPUT); //assigning the potentiometer as an input
pinMode(Step,OUTPUT); //

 pinMode(Dir,OUTPUT);
pinMode(Ab,OUTPUT);
digitalWrite(Step, LOW);
digitalWrite(Dir, LOW);
digitalWrite(Ab, HIGH);
pinMode(SW1, INPUT);
pinMode(SW2, INPUT);
pinMode(LMUP, INPUT);
pinMode(LMDW, INPUT);

}

Void loop () {

  value = analogRead(pot); /*assigning the variable "value" with the value of the potentiometer (0-1024) which is respective to (0-5v)since we have 4 leds and we want to break the potentiometer into 4 areas for each led, simply divide 1024/4 = 256, therefore every 256 increment will activate another led (256, 512, 768, 1024)  */

 if(value >= 0 && value < 125)

{

    digitalWrite (led1, LOW);

 digitalWrite (led2, LOW);
digitalWrite(led3, LOW);
digitalWrite(led4, LOW);
Vel=500;

 }

  else if(value >= 125 && value < 256){
digitalWrite(led1, HIGH);
digitalWrite(led2, LOW);
digitalWrite(led3, LOW);
digitalWrite(led4, LOW);
Vel=400;

  }

  else if(value >= 256 && value < 512){
digitalWrite(led1, HIGH);
digitalWrite(led2, HIGH);
digitalWrite(led3, LOW);
```

Void Loop ()

The majority of the code is executed inside this section. After the execution of void setup (), the loop () is initiated. The program starts right after the opening curly brace ({), and the processor executes the lines of code until it reaches the closing curly brace (}). Once at the end, it jumps back to the first line of the loop and starts over.

There are further sub loops in the program.

1. **If and Else function for potentiometer**. Assigning the potentiometer with different range of values for leds and for each range a particular value of velocity is defined. In “If function” the conditions are defined, if these conditions are true it will execute the function,

Digital Write (led1, HIGH);

This applies that, If the pin 5(LED1) has been configured as an OUTPUT with PinMode (), its voltage will be set to the corresponding value: 5V for HIGH, 0V (ground) for LOW.

```
digitalWrite(led4, LOW);
Vel=300;

  }

  else if(value >= 512 && value < 768){
digitalWrite(led1, HIGH);
digitalWrite(led2, HIGH);
digitalWrite(led3, HIGH);
digitalWrite(led4, LOW);
Vel=200;

  }

  else if(value >= 768 && value < 1024){
digitalWrite(led1, HIGH);
digitalWrite(led2, HIGH);
digitalWrite(led3, HIGH);
digitalWrite(led4, HIGH);
Vel=100;

  }

  if((digitalRead(SW1)==HIGH) && (state1==LOW))

    {

 val = digitalRead(led5);
digitalWrite(led5,!val);
digitalWrite(led6,LOW);
state1 = HIGH;

    }

 if(digitalRead(SW1)==LOW)
{
state1 = LOW;
}
if((digitalRead(SW2)==HIGH) && (state2==LOW))
{

val = digitalRead(led6);
digitalWrite(led6,!val);
digitalWrite(led5,LOW);
state2 = HIGH;
}
if(digitalRead(SW2)==LOW)
{
state2 = LOW;
}
if((digitalRead(led5)==LOW) && (digitalRead(led6)==LOW))
{
```

The **if statement** checks for a condition and executes the proceeding statement or set of statements if the condition is 'true'. Digital read function reads the value from the specified pin.

if the function reads the value of SWI (Pin 10) as High from initial LOW state(In other words Switch 1 is pressed from initial off state), then it will execute the function the function described in the brackets

If the statement described above is true then with in the curly brackets, function will read the value of Pin 11 (led5)
digital Write(led5,!val) it will turn on led 5 with SW1 in high state and logical not operator **!** will reverse its function if some other button is

Continuing the same loop if the value of the SW is Low (OFF) then the state of switch will remain LOW.

Similar explanation holds for switch 2.

```
digitalWrite(Ab,LOW);
}
if(digitalRead(led5)==HIGH)
{
digitalWrite(Dir,HIGH);
digitalWrite(Ab,HIGH);
if(digitalRead(LMUP)==HIGH)
{
digitalWrite(Ab,LOW);
}
Vel=100;
}
if(digitalRead(led6)==HIGH)
{
digitalWrite(Dir,LOW);
digitalWrite(Ab,HIGH);
if(digitalRead(LMDW)==HIGH)
{
digitalWrite(Ab,LOW);

 }
}
```

Stepper motor is controlled with three functions connected to arduinio with three pins. These are 1.**enable,** which turns on or off the stepper motor

2. **Dir,** Which decides the direction of motor movement, either clockwise or anticlockwise

3.**Step**, which controls the motion or steps of the stepper motor . Leds and Switches are integrated with motor functions. So according to program structure , motor program will function according to state of leds.

If the state of led5 and 6 are low, stepper motor will remain in low state. **Digital Write (Ab,LOW);** indicates that enable function of stepper motor is low if the states of leds is low . In other words, motor will remain off

```
digitalWrite(Step, LOW);
delayMicroseconds(Vel);
digitalWrite(Step, HIGH);
delayMicroseconds(Vel);
digitalWrite(Step, LOW);
delayMicroseconds(Vel);
digitalWrite(Step, HIGH);
delayMicroseconds(Vel);

}

}
```

Step function is actually controlling the motion of stepper motor.

It is executing the motor to move with the value described in the potentiometer function.

Delay Microseconds (Vel); is used because rotor moves very little between micro steps, and waiting time between the steps is reduced to achieve smooth function of the motor.

Appendix II

II-Data variation and Anomaly

In this experimental work, it was not always possible to get the refined results. Fluctuation in electric power consumption, variation in material removal rate and data anomalies influenced the variation in specific energy consumption values from standard ones. For this reason, only refined and good values have been used in experimental results.

II-1 Fluctuation in Electric power consumption

To determine the relationship of material removal rate with specific energy consumption, the average value of electric power consumption at each feed rate has been used to calculate the specific energy consumption. Non-uniform distribution of material grains at some places in the material, non-uniform thickness of cutting disc, vibration and further bending of cutting disc during cutting operation caused fluctuation in electric power consumption and variations in the material removal values at the same feed rate.

The fluctuation in power consumption is more prominent at lower feed rates, because the vibration in cutting discs is higher at lower feed rates. Figures presented below explain this phenomenon.

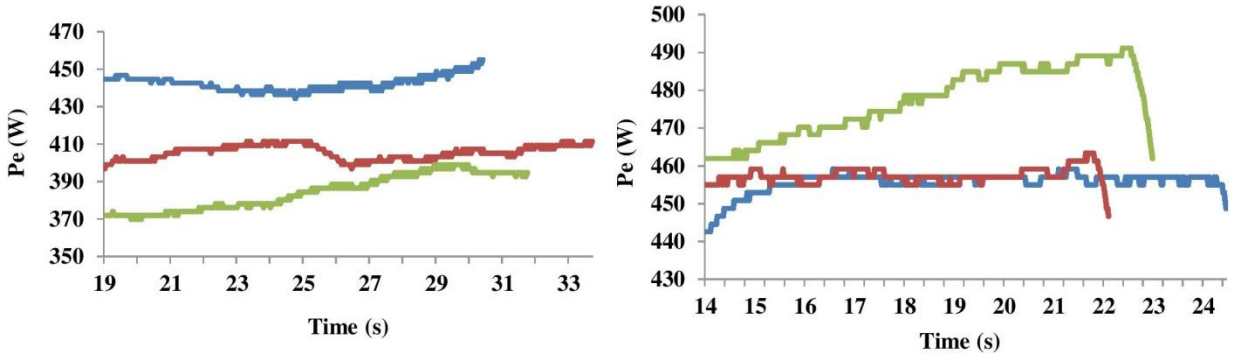

Figure 24. Electric power consumption at feed rate of 0.534 mm/s (left) and 0.613(right) for material of S235JR

In figure 24, at low material removal rates, due to , the fluctuation in electric power consumption is higher, and as a result the variations in different measurements is higher. In this case, the anomalous values are omitted while calculating average.

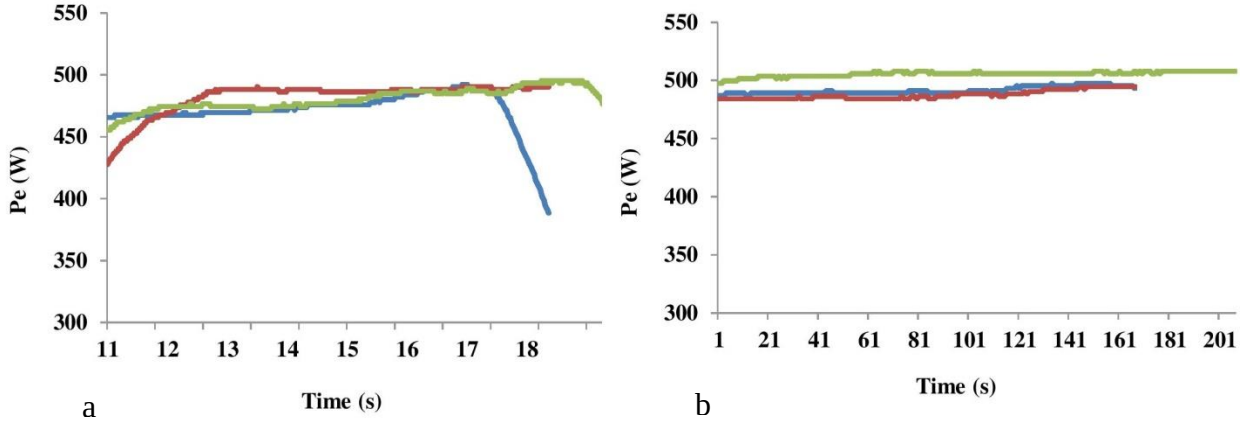

Figure 25. Electric power consumption at feed rate of 0.9mm/s(a) and 1.5 mm/s(b) for material of S235JR

Moving towards higher feed rate, the fluctuation between different measurements at the same feed rate reduced. As shown in figure 25a, that as we move towards the higher feed rates, the fluctuation and difference in electric power consumption at the same feed rate for the same material is lower in comparison for different measurements at lower feed rates in figure 24. In figure 25b, at higher feed rates, when the disc rotation stabilises, the fluctuation in power consumption among different measurements reduces to a minimum value.

II-2 Variation in material removal rate

The variation in cutting thickness along the length of cutting path is the main reason for variation in material removal rate. Figure 26 is showing two lengths at a feed rate of 0.538 for Al 1100. At point A, where disc engages with the material, the cutting thickness has found to be wider. In the middle, cutting thickness stabilizes, and it narrows down at the end. Measurements in the middle section have been used for calculating material removal rate. The corresponding table shows the variations in measurements along the cutting path.

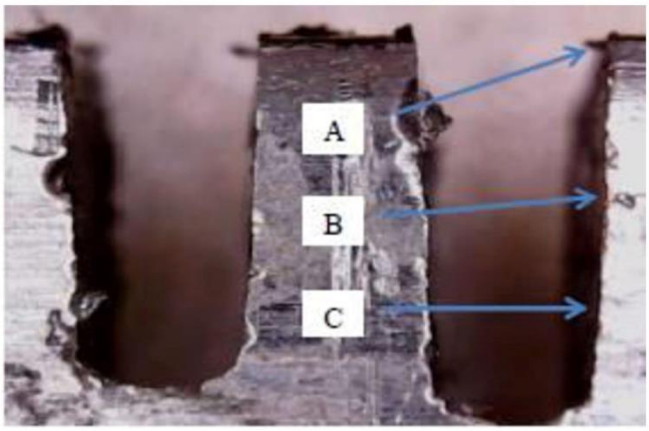

0.54 mm/s	0.54 mm/s
2.2	2.23
2.1	2.04
2.12	2.01
2.01	1.9
1.95	1.85

Figure 26. Cutting thickness variation along the length of cutting for AL 1100

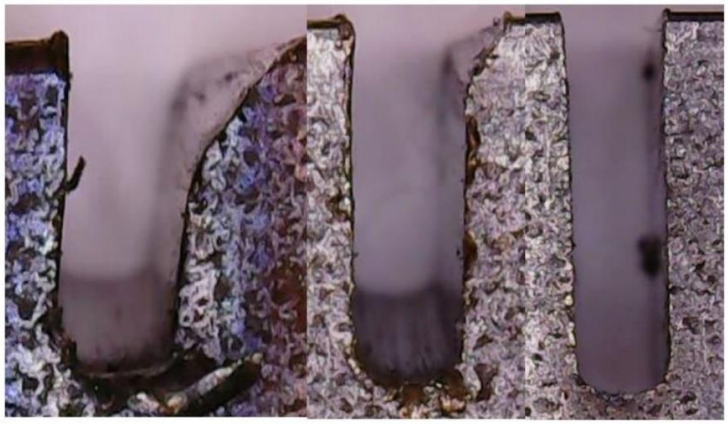

0.54 mm/s	0.64 mm/s	0.9 mm/s
2.8	2.5	1.9
2.7	2.2	1.85
2.4	1.9	1.84
2.2	1.91	1.84
2.1	1.9	1.83

(a) V_f=0.54 mm/s (b) V_f=0.64 mm/s (c) V_f=0.9 mm/s

Figure 27. Cutting thickness for C45K at different feed rates

Moving towards higher feed rates, cutting thickness became uniform for some materials. In figure 27, variation in cutting thickness for different feed rates has been shown. It can be seen that at lower feed rates, due to vibration of cutting disc, there is a large variation in cutting thickness along the length of cutting path. With increase in feed rate, for instance 0.64mm/s, this variation is reduced and at higher feed rates, cutting thickness remained almost uniform.

II-3 General Anomalies in Specific energy consumption values

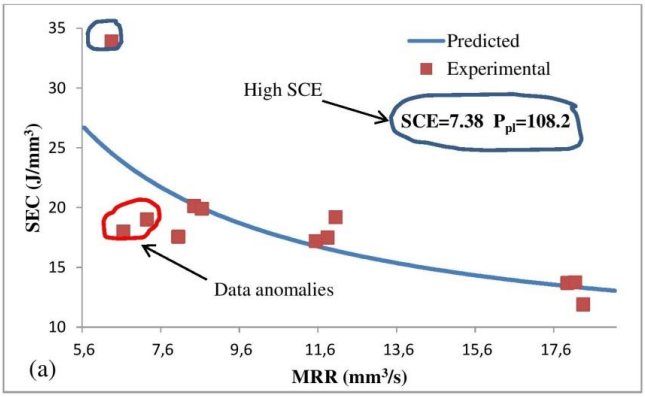

SEC (J/mm³)	Vf (mm/s)
33.9	0.54
17.8	0.54
19.0	0.54
17.6	0.64
20.1	0.64
19.9	0.64
17.5	0.9
19.2	0.9
17.2	0.9
11.9	1.5
13.7	1.5
13.7	1.5

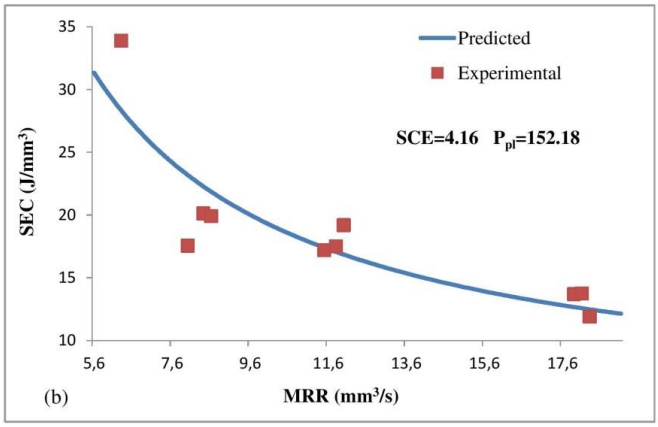

Figure 28 (a) Generally Anomaly (b) Anomaly Corrected

SEC decrease with increase in material removal rate. At low material removal rate, SEC values are higher. Data anomaly could be the low values of SEC at lower feed rate or very high values of SEC at higher feed rates. In figure 28a, at a low feed rate of 0.54mm/s, SEC values of 17.8 and 19.0 J/mm^3 are anomalies; it is not possible to have such low values at lower feed rate. Using anomalies in the data set for regression changed the coefficients of the model, which do not represent the actual value of SCE and P_{pl}. To avoid the anomaly, at each feed rate, three measurements of energy consumption are usually made, so if one or two values become anomalies, these can be omitted. In the figure 28b, performing the regression curve fitting by omitting the anomalies corrected the coefficients of the model. A better curve fitting technique of Artificial neural network (ANN) automatically detects anomalies, and does not consider them in calculation.

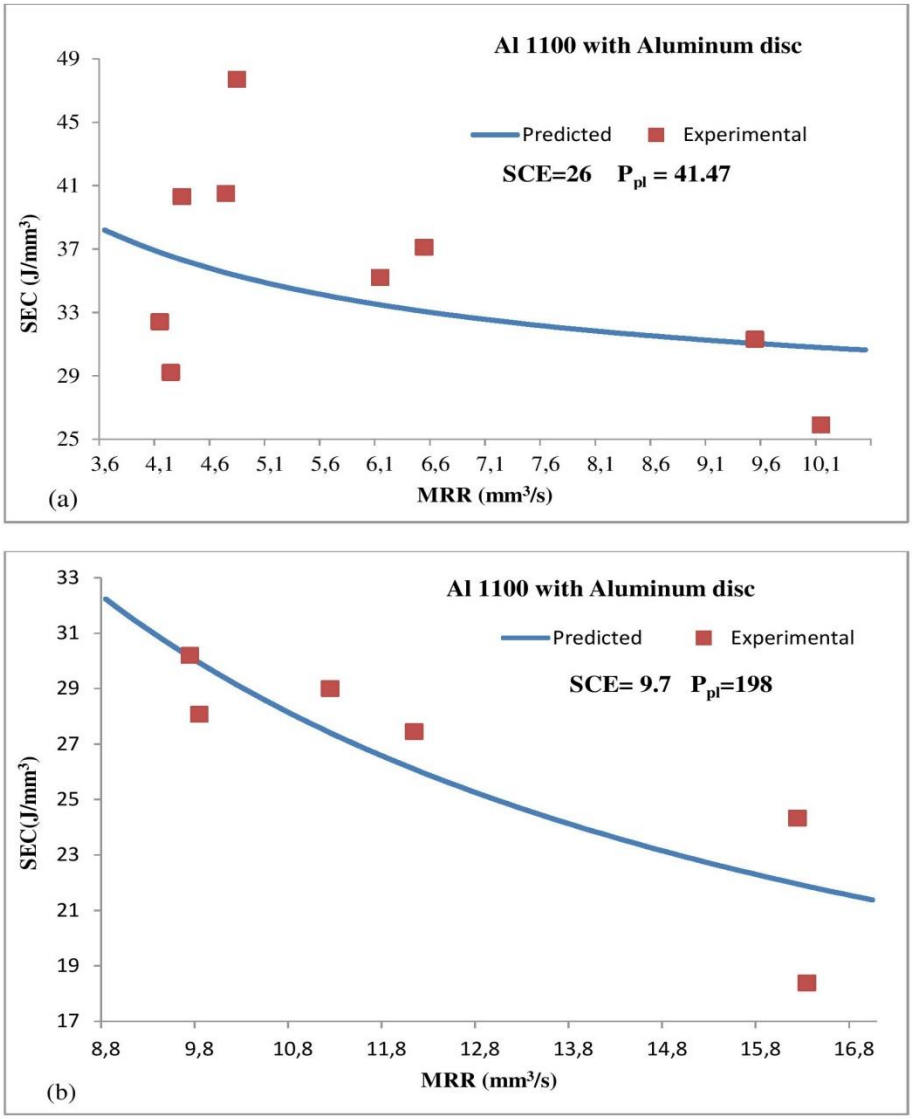

Figure 29 Anomalies due to low material removal rate (a) General anomaly (b) Anomaly omitted

II.4 Anomalies due to low material thickness

It has been found that very low material thickness for experimentation has resulted in very high SEC values that do not give the accurate representation of energy consumption. In figure 29a, SEC has been evaluated with MRR for a material thickness of 3mm. The material removal at thickness is very low, as a result, SEC is very high and behavior of the curve is not asymptotic. The SCE value is very high, due to which the curve almost tends to be straight line. Increasing the material thickness to 9mm as shown in figure 29(b), the behavior of the graph becomes asymptotic with model coefficients values of SCE and P_{pl} equal to 9.7J/mm^3 and 198 J/s respectively. This indicates that abrasive metal cutting with thin disc have a material thickness limitation. For very thin materials, model did not give the accurate representation of SEC energy consumption values. The SCE and power of plowing would likely to be affected as well.